https://doi.org/10.5194/egusphere-2026-5937
Preprint. Discussion started: 24 November 2026
© Author(s) 2026. CC BY 4.0 License.

Ecotone shifts restructure evapotranspiration and induce persistent hydrological legacy effects

Weihang Zhao [1,2,3], Yide Guo [4], Qun'ou Jiang [1,3], Linjuan He [1], Yao Xiao [1]

[1] School of Soil and Water Conservation, Beijing Forestry University, Beijing 100083, China.

[2] School of geographic Sciences, East China Normal University,Shanghai 200062, China.

[3] Key Laboratory of Soil and Water Conservation and Desertification Prevention, Beijing Forestry University, Beijing 100083, China.

[4] Department of Geography, The University of Hong Kong, Hong Kong, China

Correspondence: Qun'ou Jiang(jiangqo@bjfu.edu.cn)

Abastact. Ecotone migration alters land-surface water and energy partitioning, yet hydrology lacks a quantitative framework to distinguish immediate biophysical responses from lagged vegetation–soil adjustments. This limits prediction of evapotranspiration dynamics in regions undergoing vegetation boundary shifts. Here, we isolated the persistent hydrological legacy effects of ecotone migration along the eastern Tibetan Plateau during 1982–2020. We delineated six ecotone types using water–energy indices, simulated latent heat flux with an optimized Shuttleworth–Wallace dual-source model, and constructed a no-migration counterfactual scenario to quantify migration legacy effects on evapotranspiration. All six ecotone types underwent substantial spatial shifts, while legacy effects varied markedly among types and migration stages. Relative to the no-migration scenario, canopy transpiration increased by 1.3–17.2 W m^{-2} and soil evaporation decreased by 0.3–8.5 W m^{-2}, indicating that evapotranspiration responses were driven primarily by component redistribution rather than total flux changes. Along the humidity gradient, legacy effects

https://doi.org/10.5194/egusphere-2026-5937
Preprint. Discussion started: 24 November 2026
© Author(s) 2026. CC BY 4.0 License.

remained stable in humid ecotones but weakened or reversed in arid ecotones. Soil-moisture memory timescales ranged from 2.2 to 6.7 months, with longer memory associated with greater legacy-effect stability. These findings show that water–energy conditions, soil-moisture memory, and evapotranspiration component reorganization jointly regulate post-migration flux responses. Neglecting these lagged hydrological feedbacks may bias regional evapotranspiration estimates, particularly in high-elevation arid ecotones, where ecological restoration should account for temporal mismatches among migration, memory, and response.

Keywords: Ecotone migration; Legacy effects; Evapotranspiration partitioning; Latent heat flux; Water–energy gradient; Tibetan Plateau

1 Introduction

Ecotones are jointly shaped by water and energy availability and are among the ecological regions most sensitive to climate change (Albrich et al., 2020; Priya et al., 2023). As regional moisture–energy regimes change, ecotone boundaries identified using moisture–energy indices can respond rapidly, as manifested by their expansion, contraction, or directional migration (Zhang et al., 2022). However, the spatial displacement of an ecological boundary does not imply that the moisture and energy properties of the underlying land surface change synchronously (Brun et al., 2020). Adjustments in vegetation composition, canopy structure, rooting distribution, and soil moisture often lag behind boundary migration, typically requiring multiple growing seasons to develop and potentially persisting long after the boundary has shifted (Strohmenger et al., 2022). This temporal mismatch between rapidly changing moisture–energy boundaries and the slowly adjusting vegetation–soil system means that the hydrological effects of ecotone migration may

https://doi.org/10.5194/egusphere-2026-5937
Preprint. Discussion started: 24 November 2026
© Author(s) 2026. CC BY 4.0 License.

continue after spatial boundary displacement (Gnanamoorthy et al., 2021; Wang et al., 2023). Assessments based solely on the climatic conditions and land-surface state at the time of migration may therefore underestimate the long-term effects of ecological boundary changes on regional water cycling and surface energy partitioning (Su et al., 2024).

Latent heat flux (LH) links the terrestrial water cycle to the surface energy balance and represents an important pathway through which ecotone migration affects land–atmosphere interactions. Migration-induced changes in canopy structure, rooting distribution, and soil moisture can alter stomatal resistance, aerodynamic resistance, and plant-available water, thereby regulating canopy transpiration, soil evaporation, and their relative contributions to total LH (Khanal et al., 2024; Zhao et al., 2024). Because land-surface adjustment lags behind ecological boundary displacement and continues after migration, LH during a given period may be controlled not only by concurrent climatic conditions but also by antecedent migration processes and the land-surface states they leave behind (Zheng et al.,2025). In relatively water-abundant regions, post-migration vegetation may maintain a high capacity for water uptake and transpiration. In water-limited regions, however, enhanced vegetation water use during earlier stages may deplete limited soil water reserves, subsequently suppressing LH and potentially reversing the direction of the migration effect. The hydrological consequences of ecotone migration therefore cannot be determined solely from the immediate increase or decrease in evapotranspiration (ET) during migration. Its persistent influence on subsequent vegetation–soil water relations must also be considered (Shen et al., 2024).

Previous studies provide an important foundation for understanding this temporal mismatch. Observations of treelines worldwide have shown that, although climate warming creates favorable conditions for treeline advance, ecological boundaries respond heterogeneously across regions.

https://doi.org/10.5194/egusphere-2026-5937
Preprint. Discussion started: 24 November 2026
© Author(s) 2026. CC BY 4.0 License.

Water availability, topography, and vegetation regeneration capacity jointly constrain the translation of climatic forcing into actual land-surface change (Harsch et al., 2009). Even where warming favors woody plant establishment and recruitment, interspecific competition and community reorganization may substantially delay vegetation responses to climatic forcing (Liang et al., 2016). Meanwhile, atmospheric evaporative demand strongly constrains ET in many ecosystems, potentially exerting a greater influence than concurrent soil moisture, and this control may intensify under continued warming (Novick et al., 2016). Studies of post-drought recovery have further shown that antecedent water deficits can continue to affect subsequent carbon and water exchanges through persistent changes in soil water storage and vegetation physiological status, indicating strong history dependence in ecosystem responses (Schwalm et al., 2017). Collectively, these studies reveal the spatial heterogeneity of ecological boundary responses, temporal lags in land-surface adjustment, the sensitivity of ET to atmospheric demand, and ecosystem memory of antecedent moisture conditions. Nevertheless, the spatial migration of ecotones, persistent post-migration adjustments of the land surface, and ecosystem memory have not yet been incorporated into a unified analytical framework. Whether migration-induced changes in vegetation and soil conditions exert quantifiable effects on the direction, magnitude, and duration of subsequent LH responses beyond those caused by concurrent climatic forcing remains poorly understood.

In this study, the persistent influence of migration-induced land-surface changes arising from the lagged adjustment of the vegetation–soil system after ecological boundary displacement is defined as the legacy effect (LE) of ecotone migration. Previous research on legacy effects has focused primarily on disturbances with relatively distinct onset and termination times, such as droughts, fires, and land-cover change. Ecotone migration, by contrast, rarely occurs at a clearly

https://doi.org/10.5194/egusphere-2026-5937
Preprint. Discussion started: 24 November 2026
© Author(s) 2026. CC BY 4.0 License.

defined time and is accompanied by continuous changes in spatial location, vegetation properties, and soil conditions. Its effects on water and energy exchanges are therefore difficult to identify through a simple comparison of conditions before and after migration. Under long-term climate change, observed variations in LH within migrated pixels comprise both the direct effects of concurrent climatic change and the indirect effects of antecedent migration mediated by persistent changes in vegetation–soil conditions. Identifying the LE therefore requires a no-migration counterfactual scenario in which land-surface conditions are held at their pre-migration state while climatic conditions are allowed to vary over time. This counterfactual must then be compared with the actual migration scenario only for pixels in which ecological boundary displacement has occurred. Such an approach controls for the effects of background climate change and isolates the persistent contribution of migration-induced land-surface changes to LH.

The eastern margin of the Tibetan Plateau provides a representative natural laboratory for investigating the LE of ecotone migration. This region forms a key transition between the Tibetan Plateau and the surrounding lowlands and is characterized by pronounced moisture and energy gradients. Forest–grassland, shrubland–grassland, and desert–grassland ecotones are distributed along a continuous humid-to-arid gradient. These ecotones differ markedly in precipitation supply, energy limitation, vegetation structure, and soil moisture memory. Consequently, their migration-induced LH and ET responses may differ in direction, magnitude, and persistence. The eastern margin of the Tibetan Plateau is also a nationally important ecological security barrier and water-conservation region in China. Changes in ET directly affect how precipitation is partitioned among atmospheric recycling, soil storage, and potential runoff generation. Neglecting the persistent effects of ecotone migration may therefore systematically bias assessments of regional evaporative water

https://doi.org/10.5194/egusphere-2026-5937
Preprint. Discussion started: 24 November 2026
© Author(s) 2026. CC BY 4.0 License.

consumption, land–atmosphere feedbacks, and water-resource change.

Against this background, we developed a framework integrating long-term ecotone mapping, process-based simulation, and no-migration counterfactual analysis to quantitatively assess the LE of ecotone migration on LH across the eastern margin of the Tibetan Plateau from 1982 to 2020. First, the major ecotones were delineated using moisture–energy indices, and their spatial distributions and migration characteristics during the study period were identified. Second, LH was simulated using a parameter-optimized Shuttleworth–Wallace dual-source model and partitioned into canopy transpiration and soil evaporation. Finally, a no-migration counterfactual scenario was constructed by holding land-surface conditions at their pre-migration state while allowing climatic conditions to vary over time. This scenario was compared with the actual migration scenario, with the statistical analysis restricted to pixels that had undergone ecological boundary displacement, thereby isolating the persistent effects of migration-induced land-surface changes on LH.

This study addressed three scientific questions: (1) What spatial migration patterns have different types of ecotones across the eastern margin of the Tibetan Plateau exhibited over the past four decades? (2) How does the LE on LH vary in direction, magnitude, and persistence among ecotone types and migration stages? (3) How do background moisture–energy conditions, soil moisture memory, the redistribution of ET components, and changes in sensitivity to climatic forcing jointly regulate the LE? The central contribution of this study is to extend the conventional view of ecotones as static spatial classes by treating them as dynamic, history-dependent land surfaces. Within a unified framework, we distinguish the direct forcing of concurrent climate change from the persistent effects of migration-induced changes in vegetation–soil conditions and reveal how the LE is maintained, attenuated, or reversed along the humid-to-arid gradient. The results

https://doi.org/10.5194/egusphere-2026-5937
Preprint. Discussion started: 24 November 2026
© Author(s) 2026. CC BY 4.0 License.

provide a clearer process-based foundation for assessing ecosystem change, managing water resources, protecting ecosystems, and supporting climate-adaptation decisions in high-elevation regions.

2. Materials and methods

2.1 Study area

The study area is located in the eastern Tibetan Plateau (92.94°–106.71°E, 30.07°–38.71°N), covering approximately 8.36×10^5 km². It occupies a key transitional region between the Tibetan Plateau, the Loess Plateau, and the surrounding lowlands. The terrain is highly variable, with elevations ranging from 394 to 6264 m above sea level and a general spatial pattern of lower elevations in the southeast and higher elevations in the northwest (Fig. 1). This complex topography creates pronounced vertical zonation and considerable spatial heterogeneity in water availability, thermal conditions, and vegetation distribution (Liang et al., 2022).

The study area is influenced by both plateau and monsoonal climates and exhibits pronounced spatial gradients in moisture and thermal conditions, transitioning from humid and subhumid climates in the southeast to semiarid and arid climates in the northwest. Seasonally frozen ground and permafrost are widely distributed across the region. Freeze–thaw processes strongly affect soil water storage and release, surface runoff generation, and land–atmosphere exchanges of water and heat. Diverse land-surface types, including alpine meadows, alpine steppes, shrublands, forests, wetlands, and deserts, occur in complex spatial mosaics, forming a highly heterogeneous ecohydrological landscape (Gao et al., 2025).

The study area encompasses the headwaters and major upper-reach runoff-generating areas of

https://doi.org/10.5194/egusphere-2026-5937
Preprint. Discussion started: 24 November 2026
© Author(s) 2026. CC BY 4.0 License.

the Yellow, Yangtze, and Lancang rivers and constitutes an important ecological security barrier and water-conservation region in China. The interspersion of forests and grasslands, shrublands and grasslands, and deserts and grasslands has created extensively distributed ecotones. These ecotones are highly sensitive to changes in temperature, precipitation, and vegetation, and their spatial migration may substantially alter surface ET processes and regional patterns of water and energy transfer. The eastern margin of the Tibetan Plateau therefore provides an ideal setting for investigating ecotone migration and its effects on LH and regional water and energy exchanges.

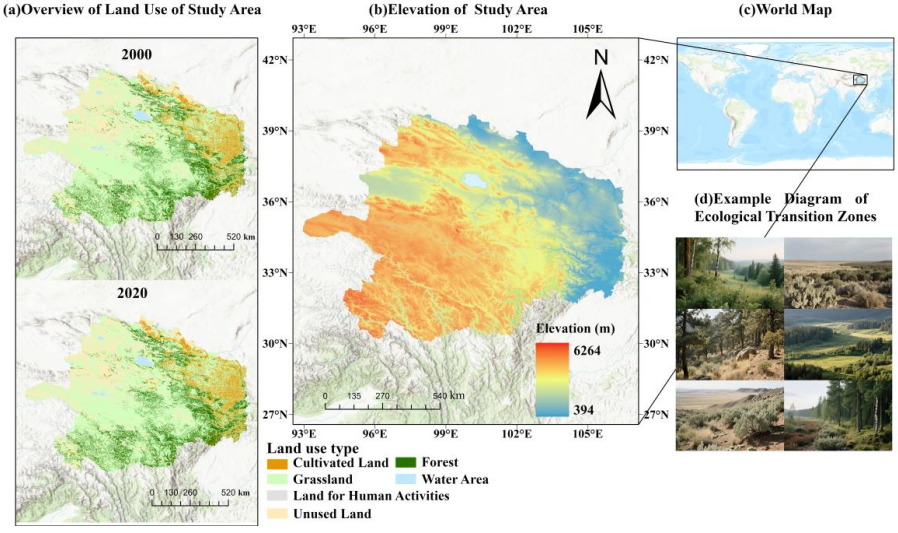

Figure 1. Geographic location, land-cover patterns, elevation, and major ecotone types in the study area. (a) Land-cover distributions in 2000 and 2020; (b) elevation; (c) global location of the study area; and (d) schematic representation of the major ecotone types.

2.2 Data sources and preprocessing

This study integrated meteorological forcing data, remotely sensed land-surface parameters, and ground-based flux observations covering the period from 1982 to 2020. Except for the site

https://doi.org/10.5194/egusphere-2026-5937
Preprint. Discussion started: 24 November 2026
© Author(s) 2026. CC BY 4.0 License.

observations used for model validation, all gridded datasets had a spatial resolution of 1 km and a monthly temporal resolution. All gridded data were clipped to the study area and aligned to a common projection and grid. Bilinear interpolation was used to resample continuous variables, whereas nearest-neighbor resampling was applied to categorical variables. During preprocessing, invalid values, observations flagged as anomalous by quality-control procedures, and pixels outside the study area were excluded. The datasets were subsequently harmonized through spatial registration and temporal matching. The processed data was used for ecotone identification, LH simulation, construction of the no-migration counterfactual scenario, and analysis of the controlling factors. The principal datasets are summarized in Table 1.

Table 1. Main datasets used in this study.

Variable/dataset	Product or source	Period	Temporal/spatial resolution
Near-surface air temperature and precipitation	National Tibetan Plateau Data Center	1982–2020	Monthly/1 km
Surface air pressure, relative humidity, and 2-m wind speed	National Earth System Science Data Center	1982–2020	Monthly/1 km
NDVI	National Earth System Science Data Center	1982–2020	Monthly/1 km
LAI	GLASS LAI	1982–2020	Monthly/1 km
Net radiation and downward shortwave radiation	GLASS land-surface parameter products	1982–2020	Monthly/1 km
Surface soil moisture	ESA CCI Soil Moisture	1982–2020	Monthly/1 km
LH observations	Arou, Daman, Zhangye Wetland, and Liancheng flux stations	2019–2020	Daily/site
Land-cover data	National Earth System Science Data Center	1982–2020	Annual/1 km

The Normalized Difference Vegetation Index (NDVI) was used to characterize vegetation activity and its temporal dynamics, while the leaf area index (LAI) was used to represent vegetation canopy structure and served as a key input for calculating canopy and boundary-layer resistances.

https://doi.org/10.5194/egusphere-2026-5937
Preprint. Discussion started: 24 November 2026
© Author(s) 2026. CC BY 4.0 License.

Net radiation (R_n) and downward shortwave radiation (DSR) were used to characterize the energy available at the land surface and incoming solar radiation, respectively. The ESA CCI surface soil moisture dataset was used to represent near-surface moisture conditions and was incorporated into the calculation of soil surface resistance, construction of the no-migration counterfactual scenario, and analysis of soil moisture memory. Land-cover data were used to identify the major land-cover types, including grasslands, croplands, wetlands, and forests, and to provide a basis for assigning model parameters to different land surfaces.

2.3 Methodology

2.3.1 Meteorological forcing

Vapor pressure deficit (VPD) is defined as the difference between the saturation vapor pressure and actual vapor pressure at a given air temperature. It characterizes atmospheric dryness and the associated atmospheric moisture demand for *ET*. In this study, saturation vapor pressure at different air temperatures was calculated using the empirical Tetens equation:

$$e^0(T) = 0.6108 \exp\left[\frac{17.27T}{T + 237.3}\right] \quad (1)$$

where T is air temperature (°C), and $e^0(T)$ is the saturation vapor pressure (kPa) at temperature T.

Because saturation vapor pressure is nonlinearly related to temperature, calculating it directly from monthly mean air temperature may underestimate the monthly mean saturation vapor pressure. To reduce this bias, saturation vapor pressure was calculated separately from the monthly mean daily maximum and minimum air temperatures and then averaged:

$$e_s = \frac{e^0(T_{max}) + e^0(T_{min})}{2} \quad (2)$$

where e_s is the monthly mean saturation vapor pressure (kPa), and T_{max} and T_{min} are the

https://doi.org/10.5194/egusphere-2026-5937
Preprint. Discussion started: 24 November 2026
© Author(s) 2026. CC BY 4.0 License.

monthly mean daily maximum and minimum air temperatures (°C), respectively.

Actual vapor pressure was calculated from monthly mean relative humidity:

$$e_a = e_s \frac{\varphi_{\text{mean}}}{100} \tag{3}$$

where e_a is the actual vapor pressure (kPa), and φ_{mean} is the monthly mean relative humidity (%). Monthly *D* was then calculated as:

$$D = e_s - e_a \tag{4}$$

where *D* is expressed in kPa. A higher *D* indicates a drier atmosphere and stronger atmospheric demand for *ET*, whereas a lower *D* indicates that the air is closer to saturation.

2.3.2 Ecotone classification and migration identification

Ecotones were classified according to the Holdridge life-zone classification system (Fan, 2021), using mean annual biotemperature (MAB), total annual precipitation (TAP), and the potential evapotranspiration ratio (PER) as moisture–energy classification indices. These indices were calculated for each 1-km grid cell and each year as follows:

$$MAB(x,y,t) = \frac{1}{n}\sum_{j=1}^{n} TEM(j,x,y,t) \tag{5}$$

$$TAP(x,y,t) = \sum_{j=1}^{n} P(j,x,y,t) \tag{6}$$

$$PER(x,y,t) = \frac{58.93 MAB(x,y,t)}{TAP(x,y,t)} \tag{7}$$

$$\begin{gathered} if\big((MAB(x,y,t) \in \{MAB_{0i}\})(TAP(x,y,t) \in \{TAP_{0i}\})(PER(x,y,t) \in \{PER_{0i}\})\big) \\ Ecotone(x,y,t) = i(1,2,3,\ldots,49); elseEcotone(x,y,t) = 0 \end{gathered} \tag{8}$$

here, $MAB(x,y,t), TAP(x,y,t)$, and $PER(x,y,t)$ represent the *MAB*, *TAP*, and *PER*, respectively, for grid cell (*x*, *y*) in year *t*. The terms MAB_{0i}, TAP_{0i}, and PER_{0i} denote the corresponding threshold ranges of biotemperature, precipitation, and *PER* for ecotone type *i*,

https://doi.org/10.5194/egusphere-2026-5937
Preprint. Discussion started: 24 November 2026
© Author(s) 2026. CC BY 4.0 License.



respectively. The continuous moisture–energy gradient was divided into 49 potential ecological types according to the different combinations of *MAB*, *TAP*, and *PER* thresholds (Appendix A). A grid cell was assigned to a given ecotone type when all three indices simultaneously satisfied the corresponding threshold criteria. Following classification, 32 types of ecotone were identified within the study area.

Based on the annual ecotone classification results, grid cells that underwent a change in ecotone type relative to the baseline state of the corresponding period were defined as migrated pixels. For each ecotone type, its area proportion, edge density, and spatial centroid were calculated. Changes in centroid location were subsequently used to determine migration distance and direction, thereby characterizing ecotone expansion, contraction, and directional displacement.

$$AP_{k,t} = \frac{A_{k,t}}{A_{study}} * 100\% \quad (9)$$

$$ED_{k,t} = \frac{L_{k,t}}{A_{study}} \quad (10)$$

where $A_{k,t}$ is the area occupied by ecotone type k in year t, A_{study} is the total study-area extent, and $L_{k,t}$ is the total boundary length of patches belonging to type k. The edge density, $ED_{k,t}$, is expressed in (m ha^{-1}). The spatial centroid of each ecotone type was calculated by weighting the coordinates of its constituent grid cells by their areas. Centroid migration distance and azimuth were derived by comparing centroid locations between adjacent years or periods, thereby characterizing the magnitude and dominant direction of ecotone migration.

2.3.3 Optimization of the Shuttleworth–Wallace model

Regional latent heat flux was estimated using an optimized Shuttleworth–Wallace (SW) dual-source model. The model partitions surface ET into two parallel sources—canopy transpiration and

https://doi.org/10.5194/egusphere-2026-5937
Preprint. Discussion started: 24 November 2026
© Author(s) 2026. CC BY 4.0 License.

soil evaporation—and can therefore represent water-vapor and energy exchanges over composite vegetation–soil surfaces (Shuttleworth et al., 1985, 1990). Total LH was calculated as:

$$LH = C_c PM_c + C_s PM_s \quad (11)$$

where LH is the total latent heat flux, and PM_c and PM_s are the latent heat fluxes under closed-canopy and bare-soil conditions, respectively. The coefficients C_c and C_s are the weighting factors for canopy transpiration and soil evaporation, respectively. The two source terms and their corresponding weighting factors were calculated as:

$$PM_c = \frac{\Delta A + \frac{\rho c_p D - \Delta r_a^c A_{soil}}{r_a^a + r_a^c}}{\Delta + \gamma \left[1 + \frac{r_s^c}{r_a^a + r_a^c}\right]} \quad (12)$$

$$PM_s = \frac{\Delta A + \frac{\left[\rho c_p D - \Delta r_a^s (A - A_{soil})\right]}{r_a^a + r_a^s}}{\Delta + \gamma \left[1 + \frac{r_s^s}{r_a^a + r_a^s}\right]} \quad (13)$$

$$C_c = \left[1 + \frac{R_c R_a}{R_s (R_c + R_a)}\right]^{-1} \quad (14)$$

$$C_s = \left[1 + \frac{R_s R_a}{R_c (R_S + R_a)}\right]^{-1} \quad (15)$$

where Δ is the slope of the saturation vapor pressure curve, A is the total available energy, and A_{soil} is the available energy at the soil surface (W m^{-2}). The parameters ρ and c_p denote air density and the specific heat capacity of air at constant pressure, respectively, and γ is the psychrometric constant. The resistance r_a^a is the aerodynamic resistance between the canopy height and the reference height, r_a^s is the aerodynamic resistance between the soil surface and the canopy, and r_a^c is the canopy boundary-layer resistance. The terms r_s^c and r_s^s represent canopy surface resistance and soil surface resistance, respectively.

To account for the heterogeneous alpine land surfaces of the Tibetan Plateau, this study adopted the parameterization scheme developed in our previous work using a combined particle swarm

https://doi.org/10.5194/egusphere-2026-5937
Preprint. Discussion started: 24 November 2026
© Author(s) 2026. CC BY 4.0 License.

optimization and genetic algorithm approach (Zhao et al., 2026). The minimum stomatal resistance, r_{smin}, and ground-surface roughness length, z_{0g}, were optimized and assigned separately by month and land-cover type, including grassland, cropland, wetland, and forest (Fig. 2). Canopy surface resistance, aerodynamic resistance, soil surface resistance, and canopy boundary-layer resistance were calculated as follows:

$$r_s^c = \frac{\mathrm{r_{smin}}}{LAIe \prod_i F_1 F_2 F_3 F_4 F_5} \tag{16}$$

$$r_a^a = \begin{cases} (\ln (x/z_0'))^2/k^2 u & h = 0 \\ \frac{1}{ku_*}\ln\left(\frac{z_a - d_0}{h - d_0}\right) + \frac{h}{nK_h}\left[\exp\left\{n\left[1 - \frac{Z_0 + d_p}{h}\right]\right\} - 1\right] & h > 0 \end{cases} \tag{17}$$

$$r_a^s = \begin{cases} 0 & h = 0 \\ \frac{hexp(n)}{nK_h} \times \left[\exp\left(-\frac{nz_{0g}}{h}\right) - \exp\left(-\frac{n(Z_0 + d_p)}{h}\right)\right] & h > 0 \end{cases} \tag{18}$$

$$r_s^s = \begin{cases} 36.821 * \theta^{-1.42} & h = 0 \\ 111.86 * \theta^{-0.58} & h > 0 \end{cases} \tag{19}$$

$$r_a^c = \frac{r_b}{2LAI} \tag{20}$$

where $LAIe$ is the effective leaf area index and r_b is the mean boundary-layer resistance (s m^{-1}). The functions F_1–F_5 represent the physiological responses of vegetation to downward shortwave radiation, D, air temperature, soil water content, and elevated atmospheric CO_2 concentration, respectively. Under bare-ground conditions, x is the reference height at which wind speed u is measured (2 m in this study), and z_0' is the aerodynamic roughness length of bare ground, fixed at 0.001 m. The parameter h is canopy height (m), k is the von Kármán constant, set to 0.41, and u_* is friction velocity (m s^{-1}). The parameter z_a is the above-canopy reference height (m), K_h is the eddy diffusion coefficient at the canopy top (m^2 s^{-1}), and n is the dimensionless decay coefficient describing the exponential decrease in eddy diffusivity within the canopy. The parameters Z_0 and d_p are the preferred roughness length and preferred zero-plane displacement height, respectively, with d_p set to 0.63h. The variable θ is volumetric soil water content (m^3 m^{-3}).

https://doi.org/10.5194/egusphere-2026-5937
Preprint. Discussion started: 24 November 2026
© Author(s) 2026. CC BY 4.0 License.

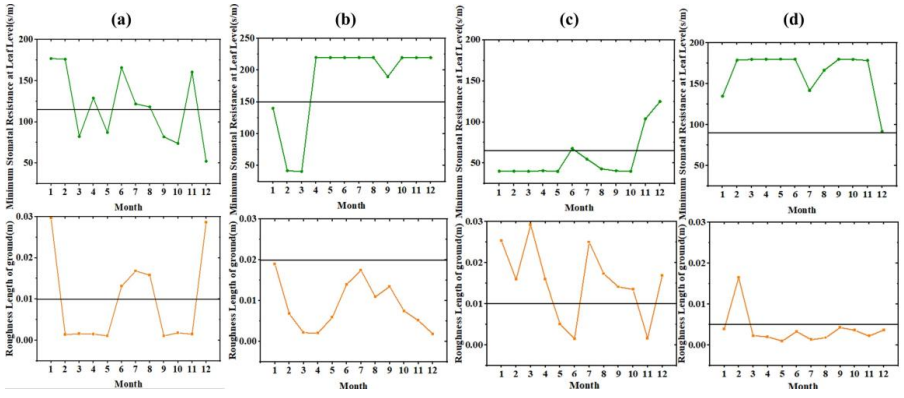

Figure 2. Monthly optimized values of minimum stomatal resistance$_{smin}$ and ground-surface roughness length z_{0g} for the major land-cover types in the study area. (a) grassland, (b) wetland, (c) cropland, and (d) forest. Black lines indicate the original parameter values before optimization.

2.3.4 Counterfactual scenario analysis and legacy-effect quantification

The legacy-effect analysis used the land-surface conditions preceding ecotone migration as the reference state. The period 1982–1991 was used to establish the initial baseline. Beginning in 1992, the study period was divided into three stages: 1992–2000, 2001–2010, and 2011–2020. For the first stage, the mean ecotone pattern and land-surface conditions during 1982–1991 were used as the baseline. For each of the subsequent two stages, the corresponding-year conditions in the preceding stage were used as the stage-specific baseline. This design enabled the LH response associated with newly occurring spatial reorganization during each stage to be quantified.

Two scenarios were constructed for each stage: an actual-migration scenario and a no-migration counterfactual scenario (Boser et al., 2024). The actual-migration scenario incorporated the contemporaneous vegetation-type parameters, LAI, NDVI, and soil moisture together with concurrent meteorological forcing, yielding LH_{obs}. In the no-migration counterfactual scenario, the

https://doi.org/10.5194/egusphere-2026-5937
Preprint. Discussion started: 24 November 2026
© Author(s) 2026. CC BY 4.0 License.

ecotone type and associated land-surface conditions were fixed at their stage-specific baseline states, while all other variables were allowed to vary over time, yielding LH_{pred}.

$$LE = \frac{LH_{obs} - LH_{pred}}{LH_{obs}} \quad (21)$$

where LE denotes the legacy effect of ecotone migration. A positive LE indicates that the post-migration land-surface state enhances LH relative to the no-migration counterfactual, whereas a negative LE indicates that it suppresses LH. All type-specific statistics were calculated exclusively for migrated pixels to prevent stable areas from diluting the legacy signal.

2.3.5 Water–energy limitations and evapotranspiration partitioning

To strengthen the hydrological interpretation of the legacy effect on LH, latent heat flux was converted into ET depth over the corresponding time interval:

$$ET = E + T = \frac{LH * \Delta t}{\lambda * \rho_w} * 1000 \quad (22)$$

where T is canopy transpiration, E is soil evaporation, and ET is the total evapotranspiration depth over the corresponding time step (mm). The terms Δt, λ, and ρ_w denote the duration of the time step (s), the latent heat of vaporization (J kg^{-1}), and water density (kg m^{-3}), respectively. Monthly ET was calculated using the actual number of days in each month, and annual ET was obtained by summing the monthly values.

To characterize the background water and energy conditions of migrated pixels across different ecotone types, the long-term mean evaporative index (EI) and soil moisture were calculated. EI was defined as:

$$EI = \frac{ET}{P} \quad (23)$$

where P is precipitation during the corresponding period. EI, PER, soil moisture, and the

https://doi.org/10.5194/egusphere-2026-5937
Preprint. Discussion started: 24 November 2026
© Author(s) 2026. CC BY 4.0 License.

standardized sensitivities of LH to environmental factors were jointly used to compare the limiting conditions at the humid and arid ends of the moisture gradient.

The SW model further partitioned total LH into canopy-transpiration and soil-evaporation components (Kool et al., 2014). For each component, the difference between the actual-migration and no-migration counterfactual scenarios was calculated as:

$$\Delta LH_T = (C_c PM_c)_{obs,t} - (C_c PM_c)_{pred,t} \quad (24)$$

$$\Delta LH_E = (C_S PM_S)_{obs} - (C_s PM_S)_{pred} \quad (25)$$

where ΔLH_T and ΔLH_E represent the differences in the LH components associated with canopy transpiration and soil evaporation, respectively, between the actual-migration and no-migration counterfactual scenarios during period *t*. Both are expressed in W m^{-2}. Positive values indicate that the corresponding ET component was enhanced under the actual-migration scenario, whereas negative values indicate that it was reduced. The ratios T/ET and E/ET were also calculated to characterize the partitioning of ecosystem water consumption among different ecotone types.

2.3.6 Environmental-driver sensitivity and soil-moisture memory

To examine the statistical relationships between deseasonalized monthly anomalies in LH and environmental factors, a multiple linear regression model was established with LH as the dependent variable and R_n, air temperature, VPD, soil moisture, precipitation, wind speed, and NDVI as independent variables. To minimize the influence of the common seasonal cycle, each variable was deseasonalized by subtracting the long-term mean for the corresponding calendar month from each monthly value:

https://doi.org/10.5194/egusphere-2026-5937
Preprint. Discussion started: 24 November 2026
© Author(s) 2026. CC BY 4.0 License.

$$X'_{y,m} = X_{y,m} - \frac{1}{N}\sum_{k=1}^{N} X_{k,m} \quad (26)$$

where $X'_{y,m}$ and $X_{y,m}$ are the anomaly and original value, respectively, for year y and calendar month m, N is the total number of years, and k is the summation index. The monthly anomaly series were subsequently winsorized at the 1st and 99th percentiles to reduce the influence of extreme values on coefficient estimation.

A multiple linear regression model was established using the deseasonalized monthly anomaly series:

$$LH'_t = \alpha + \sum_{i=1}^{p} b_i X'_{i,t} + \varepsilon_t \quad (27)$$

where LH'_t is the deseasonalized LH anomaly at time t, $X'_{i,t}$ is the anomaly of environmental driver i, b_i is the corresponding unstandardized regression coefficient, α is the intercept, ε_t is the residual term, and p is the number of environmental drivers included in the regression model.

Because the environmental variables differ in their units and ranges of variability, the unstandardized regression coefficients were converted to standardized coefficients to make them directly comparable:

$$\beta_i = b_i \frac{\sigma Xi}{\sigma LH} \quad (28)$$

where β_i is the standardized regression coefficient for environmental driver i, and σXi and σLH are the standard deviations of the corresponding environmental-driver and LH anomaly series, respectively. The sign of β_i indicates the direction of the statistical association between the environmental driver and the LH anomaly, whereas its absolute value represents the relative strength of this association after controlling for the other environmental drivers.

https://doi.org/10.5194/egusphere-2026-5937
Preprint. Discussion started: 24 November 2026
© Author(s) 2026. CC BY 4.0 License.

To further compare the relative sensitivities to different environmental drivers, the absolute standardized regression coefficients were normalized as:

$$I_{\mathrm{i}} = \frac{|\beta_i|}{\sum_{j=1}^{p}|\beta_j|} \times 100\% \tag{29}$$

where I_{i} is the normalized standardized sensitivity of LH to environmental driver *i*. This metric was used to compare the relative strengths of the statistical associations between the different environmental drivers and LH anomalies, it should not be interpreted as the proportion of LH variance independently explained by each driver. The direction of each association was determined from the sign of β_i. The I_i values for the six major ecotone types were used to compare differences in the environmental sensitivity of LH across contrasting moisture–energy regimes.

To characterize the temporal persistence of soil-moisture anomalies, the seasonal cycle and linear trend were removed from the monthly soil-moisture series for each ecotone type. Autocorrelation coefficients were then calculated at lags of 1–12 months:

$$\rho_l = \mathrm{Corr}(SM'_t, SM'_{t-l}), \qquad l = 1,2,\ldots,12 \tag{30}$$

where ρ_l is the soil-moisture autocorrelation coefficient at lag l, and SM'_t is the soil-moisture anomaly after removing the seasonal cycle and linear trend. The autocorrelation coefficients at lags of 1–12 months were used to characterize the decay of soil-moisture anomalies with increasing lag, with the lag-one autocorrelation coefficient denoted by ρ_1.

Assuming that soil-moisture anomalies approximately follow a first-order exponential decay process (Ghannam et al., 2016), the characteristic soil-moisture memory timescale was estimated from the lag-one autocorrelation coefficient:

$$\tau = \frac{-1}{\ln(\rho^1)} \tag{31}$$

where τ is the characteristic soil-moisture memory timescale, expressed in months. A largerτ indicates a slower decay and greater month-to-month persistence of soil-moisture anomalies,

https://doi.org/10.5194/egusphere-2026-5937
Preprint. Discussion started: 24 November 2026
© Author(s) 2026. CC BY 4.0 License.

whereas a smaller τ indicates a more rapid decay. The autocorrelation structure and characteristic memory timescale of each ecotone type were used to compare the persistence of soil-moisture anomalies and to provide a hydrological basis for interpreting differences in the temporal stability of migration legacy effects among ecotones.

3 Results

3.1 Validation of LH estimates from the optimized Shuttleworth–Wallace model

The model was validated using daily eddy-covariance observations of LH collected from 2019 to 2020 at four flux stations: Arou, Daman, Zhangye Wetland, and Liancheng. These stations represent grassland, cropland, wetland, and forest land surfaces, respectively. Simulated LH was matched with the station observations by date, and model performance was evaluated using the correlation coefficient (*R*) and root mean square error (*RMSE*).

The optimized Shuttleworth–Wallace dual-source model effectively reproduced the daily variations in LH across the four land-cover types, with moderate to strong correlations between the simulations and eddy-covariance observations (Fig. 3). For grassland, *R* was 0.86 and *RMSE* was 24.91 W m^{-2}. The corresponding values were 0.84 and 32.84 W m^{-2} for cropland, 0.85 and 47.63 W m^{-2} for wetland, and 0.71 and 30.54 W m^{-2} for forest. Overall, the model demonstrated satisfactory performance across the different land surfaces.

After conversion using the latent heat of vaporization, the equivalent daily ET errors for the four land-cover types ranged from approximately 0.9 to 1.7 mm d^{-1}. The errors were approximately 0.9, 1.2, 1.1, and 1.7 mm d^{-1} for grassland, cropland, forest, and wetland, respectively. Overall, the model captured both the magnitude and seasonal dynamics of LH across the different land surfaces,

https://doi.org/10.5194/egusphere-2026-5937
Preprint. Discussion started: 24 November 2026
© Author(s) 2026. CC BY 4.0 License.

providing a basis for regional LH estimation and its partitioning into canopy transpiration and soil evaporation (Zhong et al., 2021).

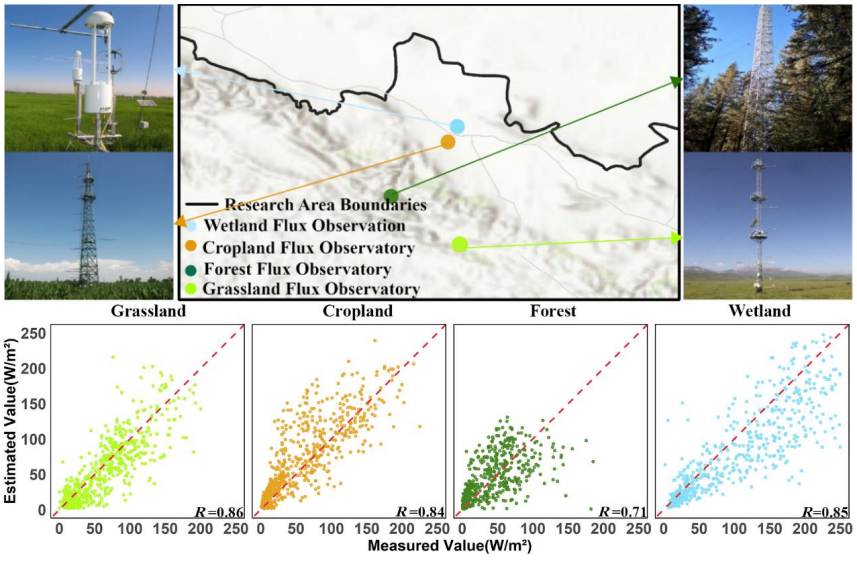

Figure 3. Distribution of flux stations in the study area and comparison between simulated and observed latent heat flux.

3.2 Spatio-temporal migration of the major ecotones on the eastern margin of the Tibetan Plateau

Based on the moisture–energy indices for the eastern Tibetan Plateau from 1982 to 2020, 32 ecotone types were identified. Six major types—the Northern Humid Forest–Cool Temperate Grassland/Humid Forest Transition Zone (NHF–CTG/HF), Northern Humid/Wet Forest–Cool Temperate Humid Forest Transition Zone (NH/WF–CTHF), Cool Temperate Humid Forest–Warm Temperate Dry/Humid Forest Transition Zone (CTHF–WTA/WF), Northern Desert/Shrub–Cool Temperate Desert Shrub Transition Zone (ND/S–CTDS), Northern Arid Shrub–Cool Temperate Desert Shrub/Grassland Transition Zone (NAS–CTDS/G), and Northern Arid Shrub/Humid Forest–

https://doi.org/10.5194/egusphere-2026-5937
Preprint. Discussion started: 24 November 2026
© Author(s) 2026. CC BY 4.0 License.

Cool Temperate Grassland Transition Zone (NAS/HF–CTG)—accounted for 67.81% of the total ecotone area and constituted the dominant components of the regional ecotone system (Fig. 4). Spatially, CTHF–WTA/WF, NH/WF–CTHF, and NHF–CTG/HF were concentrated primarily in the humid forest regions of the eastern and southeastern study area. In contrast, NAS/HF–CTG, NAS–CTDS/G, and ND/S–CTDS occurred mainly in the relatively arid northeastern and western regions. Collectively, these distributions formed a pronounced spatial gradient from the humid southeastern region toward the arid northwestern and northeastern regions.

The six major ecotone types differed markedly in their migration directions and spatial stability. NHF–CTG/HF expanded predominantly northwestward, with its proportion of the study area increasing from 0.95% to 1.77%. Its spatial position fluctuated considerably during the early study period but gradually stabilized after 2000. NH/WF–CTHF briefly expanded northeastward during the early period and subsequently retreated mainly toward the southwest. Its area proportion decreased from 1.38% to 0.85% before recovering to 1.31%, indicating a stage-dependent pattern of initial contraction followed by recovery. The overall position of CTHF–WTA/WF remained relatively stable, with only short-term displacements in certain years. However, its area fluctuated substantially during the study period and declined to approximately 0.5% by the end of the period.

The ecotones in the arid regions exhibited different spatial migration patterns. ND/S–CTDS underwent a long-term westward migration superimposed on short-term spatial fluctuations and had shifted southwestward overall by 2020. Its proportion of the study area increased from 0.21% to 0.36%. Both the spatial position and area of NAS–CTDS/G exhibited substantial interannual variability, without a persistent or consistent migration direction. Its area proportion generally ranged from 0.58% to 0.72%. NAS/HF–CTG underwent pronounced spatial changes between 1982

https://doi.org/10.5194/egusphere-2026-5937
Preprint. Discussion started: 24 November 2026
© Author(s) 2026. CC BY 4.0 License.

and 2005 and gradually stabilized thereafter. By 2020, it exhibited only a slight southeastward adjustment, while its area proportion remained within the range of 0.37%–0.52%.

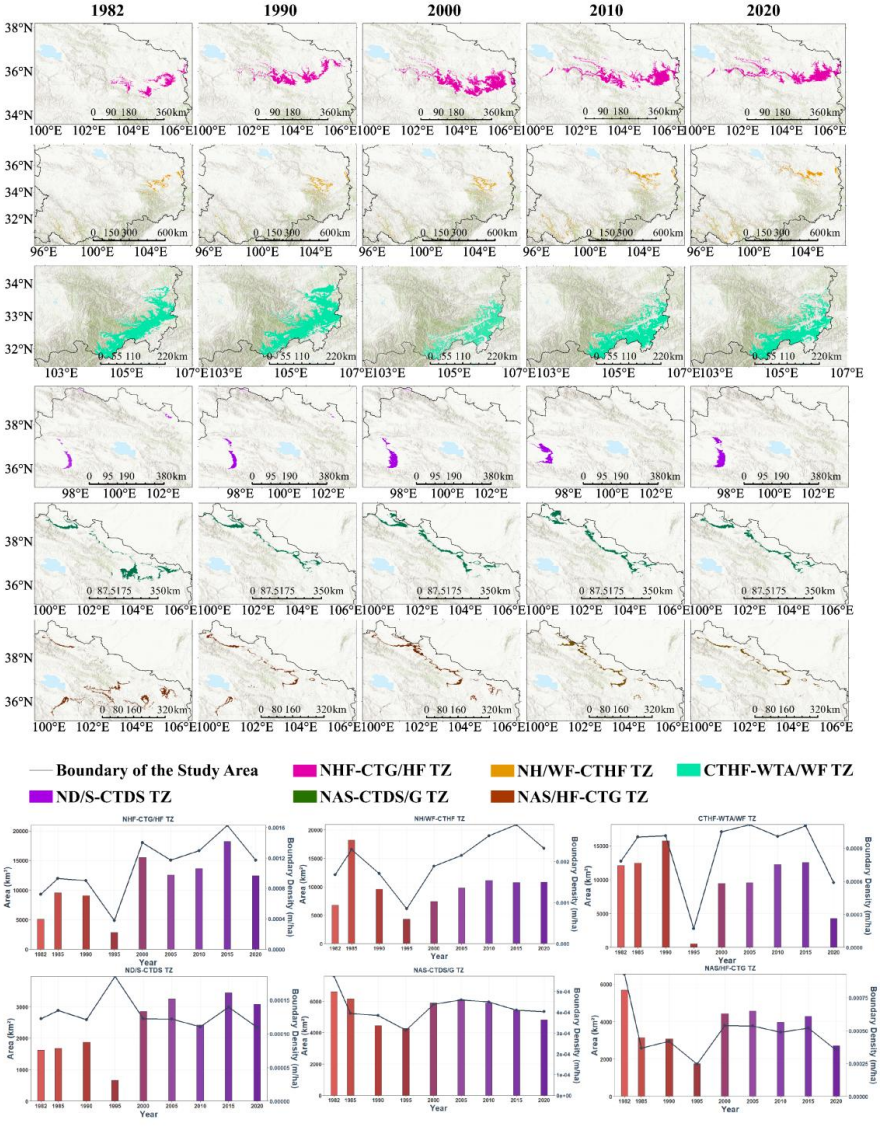

Figure 4. Spatio-temporal shifts of the six major ecotones on the eastern margin of the Tibetan Plateau from 1982 to 2020.

https://doi.org/10.5194/egusphere-2026-5937
Preprint. Discussion started: 24 November 2026
© Author(s) 2026. CC BY 4.0 License.

Overall, all six major ecotone types underwent spatial reorganization to varying degrees over the past four decades. However, these changes did not follow a uniform unidirectional migration pattern; instead, they involved different combinations of area expansion or contraction, boundary adjustment, and positional displacement. The ecotones in the humid regions exhibited expansion, retreat, or quasi-stable states, whereas those in the arid regions were characterized primarily by directional migration or frequent spatial fluctuations. These contrasting migration patterns created distinct land-surface contexts for the development of LH legacy effects among ecotone types.

3.3 Spatio-temporal nonstationarity of LH and evapotranspiration components

From 1982 to 2020, the LH across the eastern margin of the Tibetan Plateau exhibited pronounced spatial heterogeneity, with generally higher values in the southeast and lower values in the northwest (Fig. 5 and Fig. 6). LH also showed a distinct seasonal cycle. It remained at its annual minimum during winter, gradually increased in spring with rising air temperature and vegetation green-up, peaked in summer, and declined rapidly in autumn. The highest monthly mean LH, approximately 110.09 W m^{-2}, occurred in July 1994, whereas winter LH generally ranged from 7.91 to 21.98 W m^{-2}.

At the interannual scale, regional LH exhibited an overall increasing trend superimposed on substantial fluctuations. Summer peaks exceeded 100 W m^{-2} in 1994, 2006, and 2015. After 2010, the smoothed series generally remained at a relatively high level, reached a stage-specific maximum around 2014–2015, and then declined slightly. The spatial patterns and seasonal variations in ET and its components were broadly consistent with those of LH. Daily ET reached a summer maximum of approximately 3.9 mm d^{-1}, compared with approximately 0.3–0.8 mm d^{-1} during winter.

https://doi.org/10.5194/egusphere-2026-5937
Preprint. Discussion started: 24 November 2026
© Author(s) 2026. CC BY 4.0 License.

467 Analysis of LH and ET across the six major ecotone types revealed pronounced differences in
468 their multi-year mean values (Fig. 7). ND/S–CTDS had the highest mean LH, approximately 75 W
469 m^{-2}, and the greatest interannual variability, with a standard deviation of 47.17 W m^{-2}. Its multi-year
470 mean annual ET was approximately 969 mm. In contrast, NHF–CTG/HF had the lowest mean LH,
471 approximately 52 W m^{-2}, while CTHF–WTA/WF exhibited the lowest interannual variability, with
472 a standard deviation of 24.56 W m^{-2}. Except for ND/S–CTDS, the other five ecotone types had
473 relatively similar multi-year mean annual ET, ranging mainly from 668 to 705 mm.

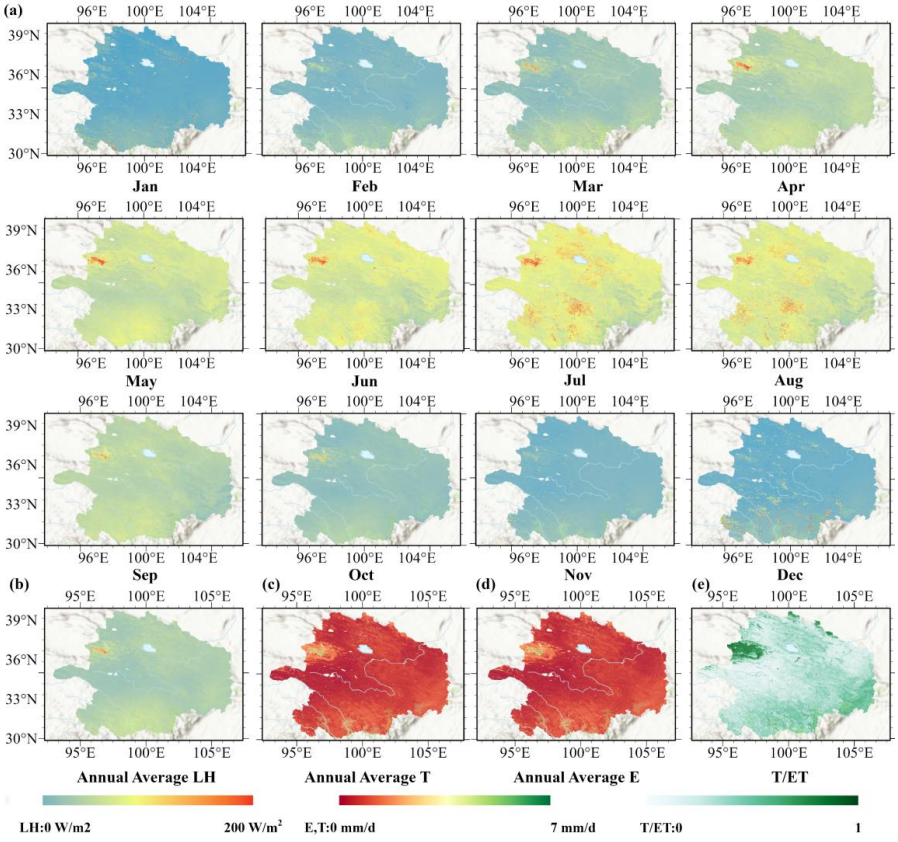

474

475 **Figure 5.** Spatial distribution of multi-year mean monthly LH and ET components across the eastern
476 margin of the Tibetan Plateau during 1982–2020. (a) Multi-year mean LH for each calendar month

https://doi.org/10.5194/egusphere-2026-5937
Preprint. Discussion started: 24 November 2026
© Author(s) 2026. CC BY 4.0 License.

from January to December; (b) multi-year mean LH; (c) multi-year mean canopy transpiration (T); (d) multi-year mean soil evaporation (E); and (e) the contribution of canopy transpiration to total ET (T/ET). LH is expressed in W m^{-2}, canopy transpiration and soil evaporation are expressed in mm d^{-1}, and T/ET is dimensionless.

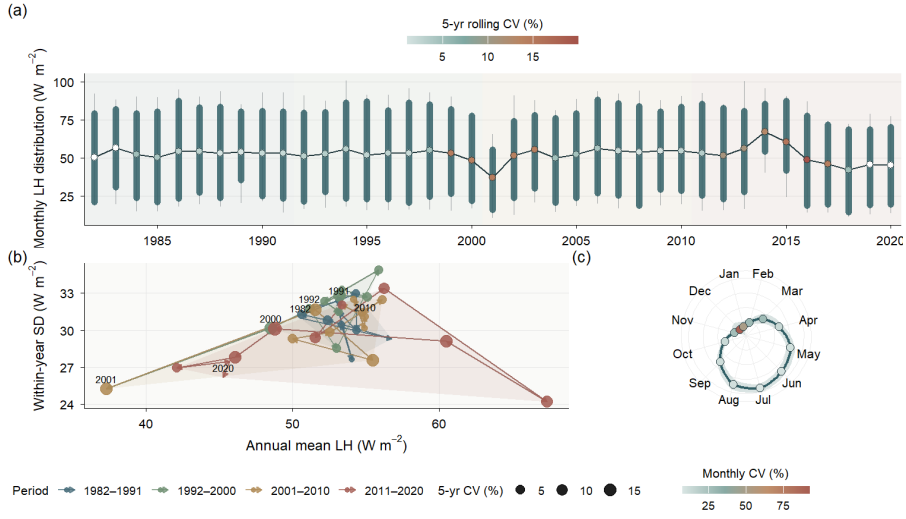

Figure 6. Interannual variability, seasonal stability, and state-space evolution of LH across the eastern margin of the Tibetan Plateau during 1982–2020. (a) Monthly LH distributions for each year and the corresponding 5-year moving coefficient of variation; (b) state-space trajectory defined by annual mean LH and the within-year standard deviation; and (c) multi-year mean seasonal cycle of LH and its monthly coefficient of variation.

Partitioning of ET into its component fluxes showed that T/ET ranged from 27% to 77% across the six ecotone types, while soil evaporation accounted for approximately 56% of total ET on average (Fig. 7b). In CTHF–WTA/WF, located at the wettest region of the moisture gradient, canopy transpiration and soil evaporation made broadly comparable contributions, with T/ET of

https://doi.org/10.5194/egusphere-2026-5937
Preprint. Discussion started: 24 November 2026
© Author(s) 2026. CC BY 4.0 License.

492 approximately 54%. The ecotones under intermediate moisture conditions were dominated by soil
493 evaporation, with T/ET ranging from approximately 27% to 38%. By contrast, the arid-end ND/S–
494 CTDS ecotone had the highest transpiration contribution, with T/ET of approximately 77% and
495 multi-year mean annual transpiration of approximately 744 mm. These results demonstrate that the
496 partitioning between canopy transpiration and soil evaporation did not vary monotonically along
497 the humid-to-arid gradient.

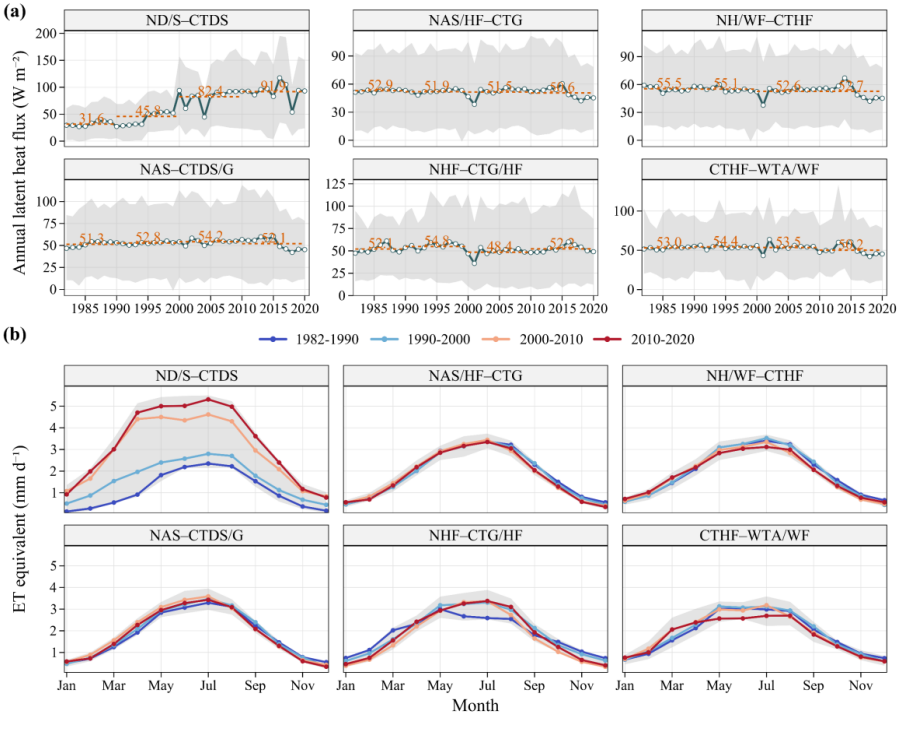

498

499 **Figure 7.** Interannual variations in LH and seasonal dynamics of ET across the six major ecotones.
500 (a) Annual mean LH, within-year minimum–maximum ranges, and period-mean values, and (b)
501 seasonal variations in ET during the four study periods. Shaded areas indicate the 10th–90th
502 percentile ranges during 1982–2020.

503

https://doi.org/10.5194/egusphere-2026-5937
Preprint. Discussion started: 24 November 2026
© Author(s) 2026. CC BY 4.0 License.

3.4 Legacy effects of ecotone migration on latent heat flux

The legacy effects of ecotone migration on LH varied markedly among ecotone types and migration stages and exhibited pronounced seasonal fluctuations (Fig. 8). When expressed as the net difference in LH between the actual-migration and no-migration counterfactual scenarios, most of the six ecotone types exhibited positive legacy effects during 1992–2000, with mean magnitudes ranging from 2.1 to 7.6. CTHF–WTA/WF, NHF–CTG/HF, and ND/S–CTDS had the largest net effects, at approximately 7.6, 7.2, and 7.0, respectively, whereas the effects for the other three ecotone types ranged from 2.1 to 2.9. These results indicate that ecotone changes during the early study stage generally enhanced LH within migrated areas.

During 2001–2010, the legacy effects diverged substantially among ecotone types. CTHF–WTA/WF and NH/WF–CTHF maintained weak positive effects of approximately 2.9 and 1.1, respectively, while NAS–CTDS/G exhibited a positive effect of approximately 1.5. In contrast, NHF–CTG/HF and NAS/HF–CTG shifted to negative effects of approximately −2.2 and −1.8, respectively. ND/S–CTDS exhibited the strongest positive response during this stage, with a net legacy effect of approximately 25.2, substantially exceeding those of the other ecotone types. This result indicates that LH in ND/S–CTDS responded particularly strongly to ecotone reorganization during this period.

During 2011–2020, the divergence in legacy effects among ecotone types became more pronounced. CTHF–WTA/WF continued to exhibit a relatively strong positive effect of approximately 7.8, whereas NH/WF–CTHF and NHF–CTG/HF showed weak positive effects of approximately 1.6 and 0.6, respectively. By contrast, NAS/HF–CTG, NAS–CTDS/G, and ND/S–CTDS exhibited negative effects of approximately −0.9, −3.6, and −6.2, respectively. The net effect

https://doi.org/10.5194/egusphere-2026-5937
Preprint. Discussion started: 24 November 2026
© Author(s) 2026. CC BY 4.0 License.

for ND/S–CTDS shifted from a strongly positive value during 2001–2010 to a negative value during 2011–2020, demonstrating a pronounced stage-dependent reversal in the legacy effect of this arid-region ecotone.

The monthly relative legacy effects further revealed distinct temporal evolution patterns among the ecotone types. CTHF–WTA/WF exhibited the most persistent positive response, with positive effects occurring in approximately 96% of months. Except for brief negative effects around 2001 and during several winter and spring months, positive effects predominated throughout the study period. The maximum relative legacy effect, approximately 0.31, occurred in June 2020. NH/WF–CTHF showed a clear seasonal contrast, with predominantly positive effects in summer and negative effects in winter, although its stage-mean net effects remained positive during all three periods.

The legacy effect for NHF–CTG/HF shifted from a relatively stable positive response during the early stage to a pronounced negative anomaly around 2001, followed by alternating weak positive and negative fluctuations. NAS/HF–CTG generally exhibited weak effects but gradually shifted toward negative values during the latter two stages. NAS–CTDS/G showed weak effects during the early stage, underwent a rapid transition from strongly positive to strongly negative values around 2000, and exhibited increasingly negative effects after 2011. Positive effects occurred in only approximately 16% of months during the late stage. ND/S–CTDS exhibited the greatest variability, progressing from negative effects during the early period to strongly positive effects during the middle period and returning to negative effects during the late period. It therefore showed the most pronounced stage-dependent reversal among the six ecotone types.

Overall, the legacy effects of the six major ecotone types can be summarized into three principal patterns. CTHF–WTA/WF exhibited a persistent and relatively stable positive effect.

https://doi.org/10.5194/egusphere-2026-5937
Preprint. Discussion started: 24 November 2026
© Author(s) 2026. CC BY 4.0 License.

NH/WF–CTHF and NHF–CTG/HF showed weak to moderate effects characterized by seasonal contrasts or stage-dependent recovery. NAS/HF–CTG, NAS–CTDS/G, and ND/S–CTDS were more likely to exhibit negative effects or directional reversals during the late stage. These findings demonstrate that the influence of ecotone migration on LH is not temporally invariant but is continuously adjusted according to ecotone type and migration stage.

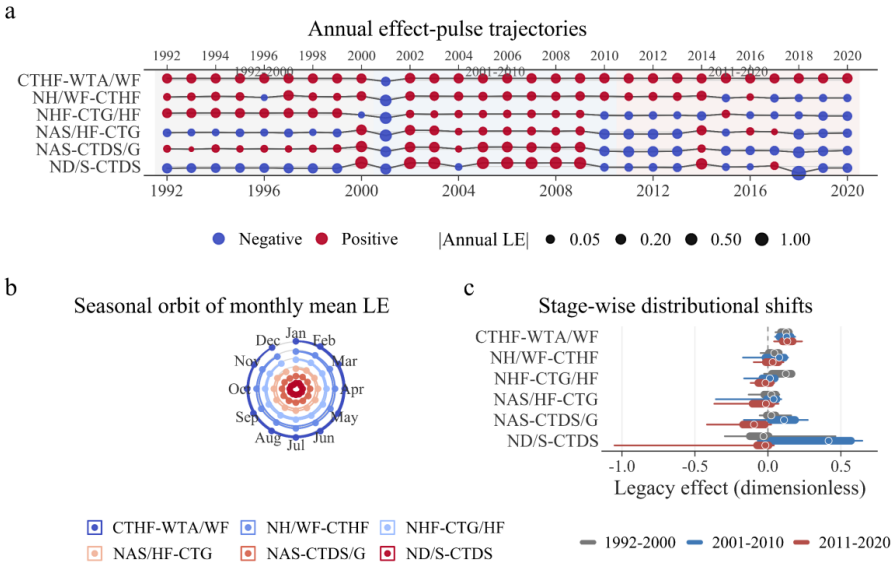

Figure 8. Temporal, seasonal, and stage-dependent variations in legacy effects across the six ecotone types. (a) Interannual variations; (b) mean monthly seasonal patterns; and (c) distributions during 1992–2000, 2001–2010, and 2011–2020.

3.5 Regulation of evapotranspiration partitioning and legacy effects by the water–energy gradient

The six major ecotone types formed a continuous water–energy gradient from humid to arid conditions (Fig. 9a). The multi-year mean evaporative index of migrated pixels increased

https://doi.org/10.5194/egusphere-2026-5937
Preprint. Discussion started: 24 November 2026
© Author(s) 2026. CC BY 4.0 License.

progressively from 0.81 in CTHF–WTA/WF to 1.22 in NH/WF–CTHF, 1.30 in NHF–CTG/HF, 2.28 in NAS/HF–CTG, and 2.98 in NAS–CTDS/G, reaching 6.65 in ND/S–CTDS. Correspondingly, mean soil moisture declined continuously from the humid CTHF–WTA/WF ecotone to 0.143 m^3 m^{-3} in the arid ND/S–CTDS ecotone.

This gradient was primarily associated with spatial differences in precipitation supply. Multi-year mean precipitation decreased by approximately 82.5%, from about 832 mm at the humid end of the gradient to about 146 mm at the arid end. In contrast, multi-year mean ET ranged mainly from 668 to 705 mm across the five ecotone types other than ND/S–CTDS. Thus, the increase in the evaporative index toward the arid end was primarily attributable to the rapid decline in precipitation rather than a concurrent increase in ET. CTHF–WTA/WF had an evaporative index below 1 and the highest soil moisture, representing the relatively water-abundant end of the gradient. All other ecotone types had evaporative indices greater than 1, accompanied by decreasing soil moisture, indicating that the imbalance between local precipitation supply and evaporative water consumption intensified toward the arid end.

Standardized regression analysis based on LH anomalies revealed systematic changes in the relative importance of environmental factors along the water–energy gradient (Fig. 9b). In humid forest ecotones, net radiation and D exhibited relatively high normalized absolute standardized coefficients, whereas the relative importance of soil moisture was only approximately 2%–4%. This indicates that the interannual variability in LH was primarily associated with variations in available energy and atmospheric evaporative demand. Toward the arid end, the relative importance of soil moisture and wind speed progressively increased. In ND/S–CTDS, the relative importance of soil moisture and wind speed reached approximately 27% and 26%, respectively, whereas that of net

https://doi.org/10.5194/egusphere-2026-5937
Preprint. Discussion started: 24 November 2026
© Author(s) 2026. CC BY 4.0 License.

radiation and D decreased. These changes were broadly consistent with the water–energy gradient indicated by the increasing evaporative index and declining soil moisture.

Decomposition of the LE into ET components showed that ecotone migration increased canopy transpiration but reduced soil evaporation across all six ecotone types, although the magnitudes of these changes differed markedly (Fig. 9c). CTHF–WTA/WF and ND/S–CTDS exhibited relatively large increases in canopy transpiration. ND/S–CTDS also showed the largest reduction in soil evaporation; however, the increase in canopy transpiration exceeded the decrease in soil evaporation, resulting in a strong positive net LE. In NH/WF–CTHF, NHF–CTG/HF, and NAS–CTDS/G, the increase in canopy transpiration and the decrease in soil evaporation largely offset each other, producing relatively weak net LE. In NAS/HF–CTG, the reduction in soil evaporation slightly exceeded the increase in canopy transpiration, resulting in a net effect close to zero or slightly negative.

https://doi.org/10.5194/egusphere-2026-5937
Preprint. Discussion started: 24 November 2026
© Author(s) 2026. CC BY 4.0 License.

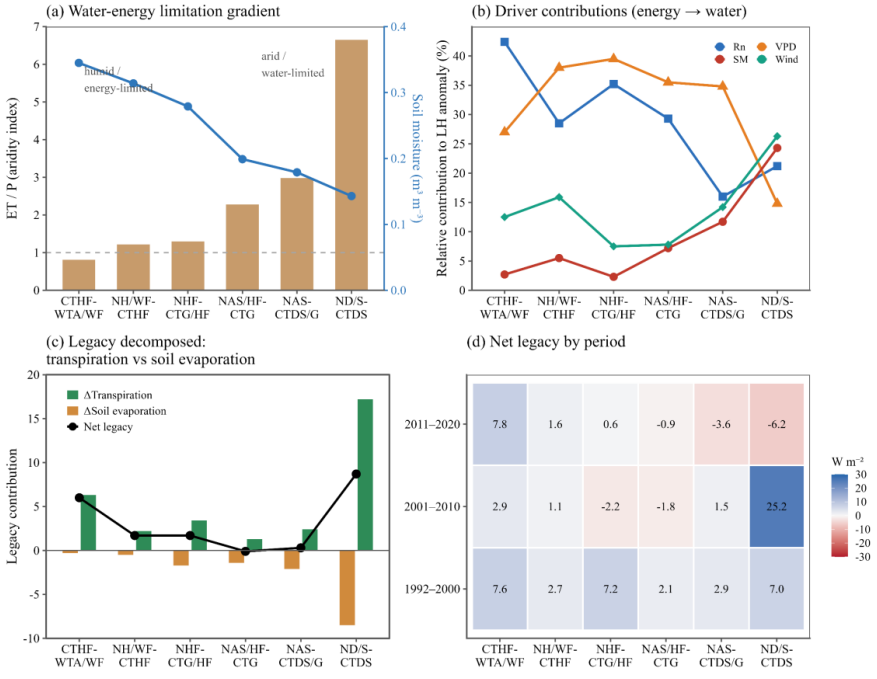

Figure 9. Water–energy controls on the evapotranspiration legacy effects of major ecotone migration along the eastern margin of the Tibetan Plateau. (a) Water–energy limitation gradient; (b) relative importance of the major climatic factors in explaining deseasonalized LH anomalies, illustrating the transition from energy limitation to water limitation along the gradient; (c) component decomposition and net legacy effects; and (d) net legacy effects on LH during different migration stages.

These results indicate that the dominant ET response to ecotone migration was not a concurrent increase or decrease in canopy transpiration and soil evaporation, but rather a redistribution of evaporative water loss from soil evaporation to canopy transpiration. The direction and magnitude of the net LE depended on whether the increase in canopy transpiration was sufficient to offset the reduction in soil evaporation, and this compensatory relationship varied with the water–energy

https://doi.org/10.5194/egusphere-2026-5937
Preprint. Discussion started: 24 November 2026
© Author(s) 2026. CC BY 4.0 License.

conditions of each ecotone.

4 Discussion

4.1 Regulation of the direction and magnitude of LE by water–energy conditions

The six major ecotone types along the eastern margin of the Tibetan Plateau formed a pronounced water–energy gradient from humid to arid conditions. The evaporative index increased from 0.81 in CTHF–WTA/WF to 6.65 in ND/S–CTDS, whereas mean soil moisture decreased from 0.345 to 0.143 $m^3\ m^{-3}$, indicating an increasing mismatch between local precipitation supply and evapotranspirative water consumption toward the arid end of the gradient (Li et al., 2019). Because some areas of the Tibetan Plateau may receive lateral water inputs, groundwater, and snow- and ice-melt water, EI was used primarily to characterize relative differences in water–energy conditions among ecotone types rather than as a stand-alone diagnostic of water limitation (Milly, 1994).

Comparison between the actual-migration and no-migration counterfactual scenarios showed positive differences in canopy transpiration for all six ecotone types, ranging from approximately 1.3 to 17.2, whereas differences in soil evaporation were consistently negative, ranging from approximately −0.3 to −8.5. These results indicate that ecotone migration was generally accompanied by a shift in the pathway of evapotranspirative water loss, characterized by enhanced canopy transpiration and reduced soil evaporation (Jiang et al., 2022). Because these two components changed in opposite directions, the magnitude of the LE depended primarily on whether the increase in transpiration could offset the decrease in soil evaporation, rather than varying monotonically along the humid–arid gradient (Feng et al.,2023).

Relatively high soil moisture at the humid end helped sustain the increase in transpiration (Cui

https://doi.org/10.5194/egusphere-2026-5937
Preprint. Discussion started: 24 November 2026
© Author(s) 2026. CC BY 4.0 License.

et al., 2020). Consequently, CTHF–WTA/WF maintained positive relative LE during all three stages, with values of approximately 0.126, 0.049, and 0.149, respectively. Although the effect weakened during the middle stage, its direction remained stable, indicating that relatively abundant water availability could buffer the additional water consumption associated with enhanced transpiration (Good et al., 2015). By contrast, in ecotones located between the humid and arid ends of the gradient, the increase in transpiration was more closely matched by the decrease in soil evaporation. Their mutual compensation resulted in relatively weak LE. For example, the relative LE values of NH/WF–CTHF during the three stages were only approximately 0.049, 0.021, and 0.022, respectively, indicating that a small net effect may mask substantial internal reorganization of ET components.

Compensation between ET components was less stable under arid conditions (Scott et al., 2021). ND/S–CTDS exhibited the largest increase in transpiration and the greatest decrease in soil evaporation. Its relative LE increased from 0.131 during 1992–2000 to 0.330 during 2001–2010, but subsequently declined to −0.061 during 2011–2020. This stage-dependent reversal suggests that enhanced transpiration during the initial period following ecotone migration may have been supported by temporarily favorable water availability but could not be sustained under persistently low soil moisture (Ma and Zhang, 2022). NAS–CTDS/G similarly exhibited a negative LE during the final stage, further demonstrating that insufficient water supply weakens the capacity of enhanced transpiration to compensate for reduced soil evaporation (Xu et al., 2021). Thus, water–energy conditions regulate the direction, magnitude, and stage-dependent stability of LE primarily by altering the balance between enhanced canopy transpiration and reduced soil evaporation (Raz-Yaseef et al., 2012).

https://doi.org/10.5194/egusphere-2026-5937
Preprint. Discussion started: 24 November 2026
© Author(s) 2026. CC BY 4.0 License.

4.2 Soil-moisture memory and the temporal persistence of LE

After removing the seasonal cycle and long-term trend, soil moisture in all six ecotone types exhibited significant month-to-month persistence. The one-month-lag autocorrelation coefficients ranged from 0.64 to 0.86, corresponding to characteristic memory timescales of 2.2–6.7 months. Such persistence reflects the finite decay of antecedent soil-moisture anomalies and is commonly characterized in terms of soil-moisture memory or persistence timescales. Differences in soil-moisture memory among ecotone types were broadly consistent with the temporal stability of their LE. NH/WF–CTHF had the longest soil-moisture memory, approximately 6.7 months. Its relative LE values during the three stages were 0.049, 0.021, and 0.022, respectively, with an interstage range of only 0.028 and consistently positive values. CTHF–WTA/WF had a memory timescale of approximately 4.9 months, and its LE was positive for approximately 96% of the study period and remained positive during all three stages. Root-zone soil-moisture memory can also vary substantially across landscape positions and hydrological settings, resulting in differences in the period over which antecedent moisture conditions remain informative (Zhang et al., 2025). These results suggest that longer soil-moisture memory can buffer short-term fluctuations in water availability caused by intermittent precipitation and transpiration water consumption.

In contrast, soil-moisture memory was substantially shorter in arid ecotones. The memory timescales of NAS–CTDS/G and ND/S–CTDS were approximately 2.2 and 2.6 months, respectively, and both exhibited pronounced stage-dependent shifts in their LE. The relative LE of NAS–CTDS/G decreased from 0.056 and 0.028 during the first two stages to −0.062 during the final stage. The relative LE of ND/S–CTDS increased from 0.131 to 0.330 before declining to −0.061, resulting in an interstage range of 0.391. Large-scale observations across China have shown that soil-moisture

https://doi.org/10.5194/egusphere-2026-5937
Preprint. Discussion started: 24 November 2026
© Author(s) 2026. CC BY 4.0 License.

memory exhibits pronounced spatial heterogeneity and that its characteristic decay timescale is particularly sensitive to meteorological conditions and evapotranspiration (Hong et al., 2026). Shorter soil-moisture memory implies a more rapid decay of antecedent soil-moisture anomalies, making LH more responsive to contemporaneous variations in precipitation, soil moisture, and atmospheric evaporative demand. The influence of soil-moisture memory on evapotranspiration also depends on the strength of the coupling between ET and soil moisture (Orth and Seneviratne, 2013). Consequently, the LE is more likely to weaken or reverse direction.

Results for ecotones occupying intermediate positions along the humid–arid gradient further indicate that soil-moisture memory is not the sole determinant of LE persistence. NHF–CTG/HF had a memory timescale of approximately 3.7 months, but its relative LE shifted from 0.126 during the early stage to −0.054 and −0.012 during the middle and final stages, respectively. NAS/HF–CTG had a memory timescale of approximately 2.3 months, and its LE likewise shifted from 0.038 to negative values. Soil-moisture memory is itself governed by interacting atmospheric, vegetation, soil, and subsurface controls, and its dominant controls may vary with temporal scale (Rahmati et al., 2024). These findings indicate that when migration-induced changes in vegetation water consumption exceed the short-term buffering capacity of soil moisture, the persistence of soil-moisture anomalies for several months is insufficient to maintain the original direction of the LE over multiple years. Recent evidence from mountain catchments further indicates that short-term soil-moisture memory is primarily associated with dynamic atmospheric forcing and vegetation processes, whereas longer-term persistence increasingly reflects slower soil and landscape controls (Zhang et al., 2026). Therefore, LE persistence at the interannual to decadal scale also depends on whether migration-induced changes in vegetation conditions, canopy parameters, and underlying

https://doi.org/10.5194/egusphere-2026-5937
Preprint. Discussion started: 24 November 2026
© Author(s) 2026. CC BY 4.0 License.

surface types persist. Soil-moisture memory provides short-term hydrological buffering, whereas persistent vegetation–soil states determine whether the resulting effects extend across multiple growing seasons.

4.3 Reorganization of evapotranspiration components and ecohydrological stability

The effects of ecotone migration on LH were reflected not only in the changes in total flux but also in a systematic reorganization of ET components. Relative to the no-migration counterfactual scenario, canopy transpiration was consistently higher under the actual-migration scenario across all six ecotone types, with differences ranging from approximately 1.3 to 17.2 W m^{-2}. In contrast, soil evaporation was consistently lower, with differences ranging from approximately −8.5 to −0.3 W m^{-2}. These persistent but opposing changes indicate that migration shifted ET partitioning toward a greater contribution from vegetation-mediated water loss relative to direct soil evaporation (Hassan et al.,2026).

Compensation between enhanced transpiration and reduced soil evaporation determined the direction and magnitude of the total LH response. On average, soil evaporation accounted for approximately 56% of total ET across the six ecotone types, indicating that it remained an important component of water consumption in the plateau ecotones. The proportion of canopy transpiration varied from approximately 27% to 77% among ecotone types, reflecting substantial differences in post-migration ET partitioning (Cao et al., 2022). When the increase in transpiration exceeded the decrease in soil evaporation, LH was higher under the actual-migration scenario than under the no-migration scenario, resulting in a positive LE. When the two changes were similar in magnitude,

https://doi.org/10.5194/egusphere-2026-5937
Preprint. Discussion started: 24 November 2026
© Author(s) 2026. CC BY 4.0 License.

their effects on total LH largely offset each other, producing an LE close to zero (Schlesinger and Jasechko, 2014). Conversely, when enhanced transpiration was insufficient to compensate for reduced soil evaporation, the LE could become negative (Fig. 10).

Ecotones occupying intermediate positions along the humid–arid gradient exhibited particularly pronounced compensation between ET components. Canopy transpiration accounted for approximately 27%–38% of total ET in NH/WF–CTHF, NHF–CTG/HF, and NAS/HF–CTG, generally lower than the corresponding proportions at the humid and most arid ends of the gradient. In these ecotones, the increase in transpiration was broadly comparable to the decrease in soil evaporation, resulting in weak or near-zero LE during some stages (Niu et al., 2019). However, a small change in total LH does not indicate that the underlying ecohydrological processes remained unchanged. Instead, it suggests that changes in total LH masked a redistribution of water consumption between vegetation and the soil surface. Assessments based solely on total ET or the net LE may therefore underestimate structural changes in subsurface-to-atmosphere water-transfer pathways (Jasechko et al., 2013).

The humid and arid ends of the gradient exhibited contrasting stability in this compensatory relationship. In CTHF–WTA/WF, canopy transpiration accounted for approximately 54% of total ET, and relatively high soil moisture supported enhanced transpiration, allowing a consistently positive LE to be maintained despite reduced soil evaporation (Chang et al., 2022). By contrast, canopy transpiration accounted for approximately 77% of total ET in ND/S–CTDS, where both the increase in transpiration and the decrease in soil evaporation were large, indicating the most pronounced reorganization of ET components. Nevertheless, its LE shifted from a strong positive value during the middle stage to a negative value during the final stage, demonstrating that a high

https://doi.org/10.5194/egusphere-2026-5937
Preprint. Discussion started: 24 November 2026
© Author(s) 2026. CC BY 4.0 License.

transpiration fraction does not necessarily correspond to a more stable LH response. Under low soil moisture and high atmospheric evaporative demand, enhanced transpiration depends more strongly on episodic water inputs. Once water supply becomes insufficient, its capacity to compensate for reduced soil evaporation may rapidly weaken.

From an ecohydrological perspective, enhanced transpiration and reduced soil evaporation indicate that a greater proportion of water is returned to the atmosphere through vegetation physiological processes rather than being lost directly from the soil surface (Ganjurjav et al., 2022). This shift may strengthen the coupling between water consumption and vegetation carbon uptake, but it should not be interpreted as necessarily reducing total water consumption or improving ecosystem stability. Here, ecohydrological stability refers specifically to the capacity of the total LH response to maintain a consistent direction and magnitude following changes in ET partitioning (Peters et al., 2018). At the humid end of the gradient, strong and persistent compensation between ET components helped maintain a consistent LH response. In the arid ecotones, however, this compensatory relationship was more sensitive to water availability and was therefore more prone to stage-dependent weakening and directional reversal. Thus, the hydrological consequences of ecotone migration depend not only on total ET but also on the relative changes in canopy transpiration and soil evaporation and the persistence of those changes.

https://doi.org/10.5194/egusphere-2026-5937
Preprint. Discussion started: 24 November 2026
© Author(s) 2026. CC BY 4.0 License.

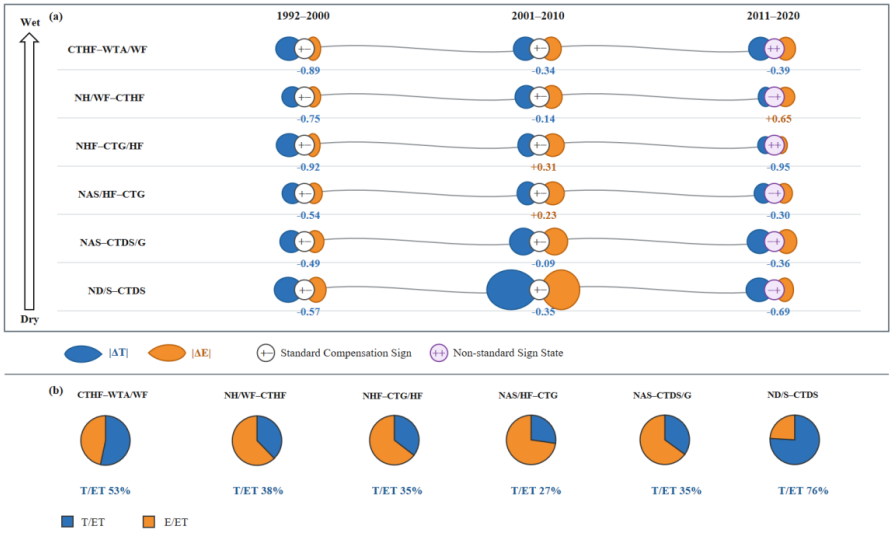

Figure 10. Stage-dependent reorganization of scenario differences in evapotranspiration components and their long-term partitioning across ecotone types. (a) Magnitudes and directions of the differences in canopy transpiration and soil evaporation between the actual-migration and no-migration counterfactual scenarios during the three stages. The blue and orange wings represent ΔT and ΔE, respectively, and the values below indicate the component-magnitude balance index. (b) Long-term proportions of canopy transpiration and soil evaporation in total ET under the actual-migration scenario during 1992–2020.

4.4 Limitations and future research

Despite the contributions of this study, several limitations should be acknowledged. First, the analysis were conducted at a spatial resolution of 1 km and a monthly temporal step, and it cannot adequately resolve fine-scale topographic heterogeneity or local-scale water–energy coupling within ecotones under the complex topographic conditions of the Tibetan Plateau. Second, our investigation targeted six dominant ecotone types that together cover a substantial portion of the

https://doi.org/10.5194/egusphere-2026-5937
Preprint. Discussion started: 24 November 2026
© Author(s) 2026. CC BY 4.0 License.

study region; however, less widespread ecotone types were not included, leaving their migration trajectories and associated hydrological responses unexplored. Third, the empirical findings are derived from a single alpine region with a pronounced humidity gradient, and it remains unclear whether similar legacy effects emerge in ecotones under contrasting climatic regimes or across different landscape settings. Comparative analyses in diverse geographic contexts are therefore needed to test the generality of our conclusions. Looking ahead, several priorities merit attention: incorporating higher-resolution remote-sensing products and in situ observations to better capture sub-grid variability, expanding the taxonomic and geographic coverage of ecotone types, and extending the analytical framework to other ecotone-prone regions to establish whether the component-driven legacy effects identified here represent a broader hydrological phenomenon.

5 Conclusions

By integrating multi-source remote-sensing data, meteorological data, and ground-based flux observations from 1982 to 2020, this study combined an optimized Shuttleworth–Wallace dual-source model with a no-migration counterfactual scenario to systematically quantify the legacy effects of ecotone migration on latent heat flux along the eastern margin of the Tibetan Plateau and the underlying hydrological controls. The main conclusions are as follows:

(1) All major ecotone types underwent pronounced spatial shifts over the past four decades, but the directions and magnitudes of these shifts varied among ecotone types, suggesting that climate warming does not uniformly drive ecological boundaries unidirectionally toward higher elevations or latitudes. Regional latent heat flux generally exhibited a southeast-to-northwest decreasing spatial pattern, together with pronounced seasonal cycles and interannual variability.

https://doi.org/10.5194/egusphere-2026-5937
Preprint. Discussion started: 24 November 2026
© Author(s) 2026. CC BY 4.0 License.

(2) The legacy effects of ecotone migration exhibited clear gradient-dependent and stage-dependent variations along the humid–arid gradient. In the humid CTHF–WTA/WF ecotone, the latent heat flux response remained positive and relatively stable throughout all three stages. In contrast, the relative legacy effect in the arid ND/S–CTDS ecotone increased from 0.131 during 1992–2000 to 0.330 during 2001–2010, then reversed to −0.061 during 2011–2020, indicating a pronounced stage-dependent transition. These contrasting behaviors were closely associated with the water–energy conditions of the ecotones. From the humid to the arid ecotone of the gradient, the evaporative index increased from 0.81 to 6.65, whereas soil moisture decreased from 0.345 to 0.143 $m^3\ m^{-3}$, indicating a progressively intensifying mismatch between precipitation supply and evapotranspirative water consumption.

(3) Relative to the no-migration scenario, canopy transpiration increased by 1.3–17.2 W m^{-2} across the six ecotones, whereas soil evaporation decreased by 0.3–8.5 W m^{-2}. Thus, the hydrological consequence of ecotone migration was not a concurrent enhancement or suppression of total evapotranspiration, but rather a fundamental redistribution of the dominant pathway by which water returns to the atmosphere—from soil surface to vegetation canopy. The direction and magnitude of the legacy effect depended on the compensation between enhanced transpiration and reduced soil evaporation. Relatively stable compensation between these components in the humid ecotones helped maintain the latent heat flux response, whereas low soil moisture in the arid ecotones increased the likelihood of effect attenuation and directional reversal.

(4) The characteristic soil-moisture memory timescales of the six ecotones ranged from 2.2 to 6.7 months. Longer soil-moisture memory in humid ecotones corresponded to relatively stable legacy effects, whereas shorter memory in arid ecotones was accompanied by more pronounced

https://doi.org/10.5194/egusphere-2026-5937
Preprint. Discussion started: 24 November 2026
© Author(s) 2026. CC BY 4.0 License.

stage-dependent transitions. These results indicate that soil-moisture memory provides an important hydrological buffer for the short-term persistence of legacy effects, whereas their persistence over multiple years depends on the joint evolution of post-migration vegetation and soil conditions.

Overall, the legacy effects of ecotone migration on latent heat flux reflect the interacting influences of water–energy conditions, soil-moisture memory, and the reorganization of evapotranspiration components. The integrated framework developed here, combining the identification of ecotone migration, process-based modelling, and legacy-effect analysis, provides a new perspective for understanding the long-term effects of dynamic ecological-boundary shifts on evapotranspiration and terrestrial water–energy exchanges in alpine regions. The findings also provide a process-based basis for water-resource management and climate-change adaptation on the Tibetan Plateau.

https://doi.org/10.5194/egusphere-2026-5937
Preprint. Discussion started: 24 November 2026
© Author(s) 2026. CC BY 4.0 License.

Appendix A

Table A1 Ecotone classification based on hydrothermal indicators

Encoding	Types of Ecological Transition Zones	*MAB(℃)*	*TAP(mm)*	*PER*
1	Aeolian Desert–Snow/Ice Transition Zone	> 0.375	< 125	< 0.25
2	Aeolian Desert–Periglacial/Snow–Ice Transition Zone	< 0.75	> 125	> 0.25
3	Aeolian Desert–Frigid Desert/Periglacial Transition Zone	> 0.75	< 125	< 0.50
4	Periglacial–Snow/Ice Transition Zone	> 0.75	< 250	< 0.25
5	Frigid Desert–Periglacial/Alpine Grassland Transition Zone	< 1.50	> 125	> 0.50
6	Periglacial–Snow/Ice and Alpine Meadow Transition Zone	< 1.50	> 250	> 0.25
7	Frigid Desert–Alpine Desert/Grassland Transition Zone	> 1.50	< 125	< 1.00
8	Periglacial–Alpine Grassland/Meadow Transition Zone	> 1.50	< 250	< 0.50
9	Snow/Ice–Alpine Meadow/Tundra Transition Zone	> 1.50	< 500	< 0.25
10	Alpine Desert/Grassland–Arid Shrub Transition Zone	< 3.00	> 125	> 1.00
11	Alpine Grassland/Meadow–Northern Humid Forest Transition Zone	< 3.00	> 250	> 0.50
12	Alpine Meadow/Tundra–Northern Wet Forest Transition Zone	< 3.00	> 500	> 0.25
13	Alpine Desert–Northern Desert/Arid Shrub Transition Zone	> 3.00	< 125	< 2.00
14	Alpine Grassland–Northern Arid Shrub/Humid Forest Transition Zone	> 3.00	< 250	< 1.00
15	Alpine Meadow–Northern Humid/Wet Forest Transition Zone	> 3.00	< 500	< 0.50
16	Northern Wet Forest/Rainforest–Tundra Transition Zone	> 3.00	< 1000	< 0.25
17	Northern Desert/Shrub–Cool Temperate Desert Shrub Transition Zone	< 6.00	> 125	> 2.00
18	Northern Arid Shrub/Humid Forest–Cool Temperate Grassland Transition Zone	< 6.00	> 250	> 1.00
19	Northern Humid/Wet Forest–Cool Temperate Humid Forest Transition Zone	< 6.00	> 500	> 0.50
20	Northern Wet Forest/Rainforest–Cool Temperate Wet Forest Transition Zone	< 6.00	> 1000	> 0.25
21	Northern Desert–Cool Temperate Desert/Shrub Transition Zone	> 6.00	< 125	< 4.00
22	Northern Arid Shrub–Cool Temperate Desert Shrub/Grassland Transition Zone	> 6.00	< 250	< 2.00
23	Northern Humid Forest–Cool Temperate Grassland/Humid Forest Transition Zone	> 6.00	< 500	< 1.00

https://doi.org/10.5194/egusphere-2026-5937
Preprint. Discussion started: 24 November 2026
© Author(s) 2026. CC BY 4.0 License.

24	Northern Wet Forest–Cool Temperate Humid/Wet Forest Transition Zone	> 6.00	< 1000	< 0.50
25	Northern Rainforest–Cool Temperate Wet Forest/Rainforest Transition Zone	> 6.00	< 2000	< 0.25
26	Cool Temperate Desert/Shrub–Warm Temperate Desert Shrub Transition Zone	< 12.00	> 125	> 4.00
27	Cool Temperate Desert Shrub/Grassland–Warm Temperate Thorn Steppe Transition Zone	< 12.00	> 250	> 2.00
28	Cool Temperate Grassland/Humid Forest–Warm Temperate Dry Forest Transition Zone	< 12.00	> 500	> 1.00
29	Cool Temperate Humid/Wet Forest–Warm Temperate Humid Forest Transition Zone	< 12.00	> 1000	> 0.50
30	Cool Temperate Wet Forest/Rainforest–Warm Temperate Wet Forest Transition Zone	< 12.00	> 2000	> 0.25
31	Cool Temperate Desert–Warm Temperate Desert/Shrub Transition Zone	> 12.00	< 125	< 8.00
32	Cool Temperate Desert Shrub–Warm Temperate Desert Shrub/Thorn Steppe Transition Zone	> 12.00	< 250	< 4.00
33	Cool Temperate Grassland–Warm Temperate Thorn Steppe/Dry Forest Transition Zone	> 12.00	< 500	< 2.00
34	Cool Temperate Humid Forest–Warm Temperate Dry/Humid Forest Transition Zone	> 12.00	< 1000	< 1.00
35	Cool Temperate Wet Forest–Warm Temperate Humid/Wet Forest Transition Zone	> 12.00	< 2000	< 0.50
36	Cool Temperate Rainforest–Warm Temperate Wet Forest/Rainforest Transition Zone	> 12.00	< 4000	< 0.25
37	Subtropical Desert/Shrub–Tropical Desert Shrub Transition Zone	< 24.00	> 125	> 8.00
38	Subtropical Shrub/Thorn Steppe–Tropical Thorn Woodland Transition Zone	< 24.00	> 250	> 4.00
39	Subtropical Thorn Woodland/Dry Forest–Tropical Very Dry Forest Transition Zone	< 24.00	> 500	> 2.00
40	Subtropical Dry/Humid Forest–Tropical Dry Forest Transition Zone	< 24.00	> 1000	> 1.00
41	Subtropical Humid/Wet Forest–Tropical Humid Forest Transition Zone	< 24.00	> 2000	> 0.50
42	Subtropical Wet Forest/Rainforest–Tropical Wet Forest Transition Zone	< 24.00	> 4000	> 0.25
43	Subtropical Desert–Tropical Desert/Shrub Transition Zone	> 24.00	< 125	< 16.00
44	Subtropical Desert Shrub–Tropical Desert Shrub/Thorn Woodland Transition Zone	> 24.00	< 250	< 8.00

https://doi.org/10.5194/egusphere-2026-5937
Preprint. Discussion started: 24 November 2026
© Author(s) 2026. CC BY 4.0 License.

45	Subtropical Thorn Woodland–Tropical Thorn Woodland/Very Dry Forest Transition Zone	> 24.00	< 500	< 4.00
46	Subtropical Dry Forest–Tropical Very Dry/Dry Forest Transition Zone	> 24.00	< 1000	< 2.00
47	Subtropical Humid Forest–Tropical Dry/Humid Forest Transition Zone	> 24.00	< 2000	< 1.00
48	Subtropical Wet Forest–Tropical Humid/Wet Forest Transition Zone	> 24.00	< 4000	< 0.50
49	Subtropical Rainforest–Tropical Wet Forest/Rainforest Transition Zone	> 24.00	< 8000	< 0.25

826

https://doi.org/10.5194/egusphere-2026-5937
Preprint. Discussion started: 24 November 2026
© Author(s) 2026. CC BY 4.0 License.

References

Albrich, K., Rammer, W., Seidl, R., 2020. Climate change causes critical transitions and irreversible alterations of mountain forests. Glob. Change Biol. 26 (7), 4013–4027.

Boser, A., Caylor, K., Larsen, A., Pascolini-Campbell, M., Reager, J.T., Carleton, T., 2024. Field-scale crop water consumption estimates reveal potential water savings in California agriculture. Nat. Commun. 15, 2366.

Brun, P., Thuiller, W., Chauvier, Y., Pellissier, L., Wüest, R.O., Wang, Z., Zimmermann, N.E., 2020. Model complexity affects species distribution projections under climate change. J. Biogeogr. 47 (1), 130–142.

Cao, R., Huang, H., Wu, G., Han, D., Jiang, Z., Di, K., Hu, Z., 2022. Spatiotemporal variations in the ratio of transpiration to evapotranspiration and its controlling factors across terrestrial biomes. Agric. For. Meteorol. 321, 108984.

Chang, Y., Ding, Y., Zhang, S., Qin, J., Zhao, Q., 2022. Dynamics and environmental controls of evapotranspiration for typical alpine meadow in the northeastern Tibetan Plateau. J. Hydrol. 612, 128282.

Cui, J., Tian, L., Wei, Z., Huntingford, C., Wang, P., Cai, Z., Ma, N., Wang, L., 2020. Quantifying the controls on evapotranspiration partitioning in the highest alpine meadow ecosystem. Water Resour. Res. 56 (4), e2019WR024815.

Fan, Z., 2021. Spatial identification and scenario simulation of ecotone distribution in China. Acta Geogr. Sin. 76 (3), 626–644.

Feng, J., Zhang, K., Zhan, H., Chao, L., 2023. Improved soil evaporation remote sensing retrieval algorithms and associated uncertainty analysis on the Tibetan Plateau. Hydrol. Earth Syst. Sci.

https://doi.org/10.5194/egusphere-2026-5937
Preprint. Discussion started: 24 November 2026
© Author(s) 2026. CC BY 4.0 License.



27, 363–383.

Ganjurjav, H., Hu, G., Zhang, Y., Gornish, E.S., Yu, T., Gao, Q., 2022. Warming tends to decrease ecosystem carbon and water use efficiency in dissimilar ways in an alpine meadow and a cultivated grassland in the Tibetan Plateau. Agric. For. Meteorol. 323, 109079.

Gao, Z., Zhang, C., Liu, W., Niu, F., Wang, Y., Lin, Z., Yin, G., Ding, Z., Shang, Y., Luo, J., 2025. Extreme degradation of alpine wet meadow decelerates soil heat transfer by preserving soil organic matter on the Qinghai–Tibet Plateau. J. Hydrol. 653, 132748.

Ghannam, K., Nakai, T., Paschalis, A., Oishi, C.A., Kotani, A., Igarashi, Y., Kumagai, T., Katul, G.G., 2016. Persistence and memory timescales in root-zone soil moisture dynamics. Water Resour. Res. 52 (2), 1427–1445.

Gnanamoorthy, P., Song, Q., Zhao, J., Zhang, Y., Liu, Y., Zhou, W., Sha, L., Fan, Z., Deb Burman, P.K., 2021. Altered albedo dominates the radiative forcing changes in a subtropical forest following an extreme snow event. Glob. Change Biol. 27 (23), 6192–6205.

Good, S.P., Noone, D., Bowen, G., 2015. Hydrologic connectivity constrains partitioning of global terrestrial water fluxes. Science 349 (6244), 175–177.

Harsch, M.A., Hulme, P.E., McGlone, M.S., Duncan, R.P., 2009. Are treelines advancing? A global meta-analysis of treeline response to climate warming. Ecol. Lett. 12 (10), 1040–1049.

Hassan, A., Prentice, I.C., Liang, X., 2026. Insights into evapotranspiration partitioning based on hydrological observations using the generalized proportionality hypothesis. Hydrol. Earth Syst. Sci. 30, 317–341.

Hong, X., Jia, S., Zhu, W., 2026. Characteristics and influencing factors of soil moisture memory across mainland China. J. Hydrol. 671, 135281. https://doi.org/10.1016/j.jhydrol.2026.135281.

https://doi.org/10.5194/egusphere-2026-5937
Preprint. Discussion started: 24 November 2026
© Author(s) 2026. CC BY 4.0 License.



871 Jasechko, S., Sharp, Z.D., Gibson, J.J., Birks, S.J., Yi, Y., Fawcett, P.J., 2013. Terrestrial water fluxes
872 dominated by transpiration. Nature 496, 347–350. https://doi.org/10.1038/nature11983.
873 Jiang, F., Xie, X., Wang, Y., Liang, S., Zhu, B., Meng, S., Zhang, X., Chen, Y., Liu, Y., 2022.
874 Vegetation greening intensified transpiration but constrained soil evaporation on the Loess
875 Plateau. J. Hydrol. 614, 128514. https://doi.org/10.1016/j.jhydrol.2022.128514.
876 Khanal, P., Hoek Van Dijke, A.J., Schaffhauser, T., Li, W., Paulus, S.J., Zhan, C., Orth, R., 2024.
877 Relevance of near-surface soil moisture vs. terrestrial water storage for global vegetation
878 functioning. Biogeosciences 21, 1533–1547. https://doi.org/10.5194/bg-21-1533-2024.
879 Kool, D., Agam, N., Lazarovitch, N., Heitman, J.L., Sauer, T.J., Ben-Gal, A., 2014. A review of
880 approaches for evapotranspiration partitioning. Agric. For. Meteorol. 184, 56–70.
881 https://doi.org/10.1016/j.agrformet.2013.09.003.
882 Li, X., Long, D., Han, Z., Scanlon, B.R., Sun, Z., Han, P., Hou, A., 2019. Evapotranspiration
883 estimation for Tibetan Plateau headwaters using conjoint terrestrial and atmospheric water
884 balances and multisource remote sensing. Water Resour. Res. 55 (11), 8608–8630.
885 https://doi.org/10.1029/2019WR025196.
886 Liang, E., Wang, Y., Piao, S., Lu, X., Camarero, J.J., Zhu, H., Zhu, L., Ellison, A.M., Ciais, P.,
887 Peñuelas, J., 2016. Species interactions slow warming-induced upward shifts of treelines on
888 the Tibetan Plateau. Proc. Natl. Acad. Sci. U.S.A. 113 (16), 4380 – 4385.
889 https://doi.org/10.1073/pnas.1520582113.
890 Liang, Y., Song, W., 2022. Integrating potential ecosystem services losses into ecological risk
891 assessment of land use changes: A case study on the Qinghai-Tibet Plateau. J. Environ. Manage.
892 318, 115607. https://doi.org/10.1016/j.jenvman.2022.115607.

https://doi.org/10.5194/egusphere-2026-5937
Preprint. Discussion started: 24 November 2026
© Author(s) 2026. CC BY 4.0 License.



Ma, N., Zhang, Y., 2022. Increasing Tibetan Plateau terrestrial evapotranspiration primarily driven by precipitation. Agric. For. Meteorol. 317, 108887. https://doi.org/10.1016/j.agrformet.2022.108887.

Milly, P.C.D., 1994. Climate, soil water storage, and the average annual water balance. Water Resour. Res. 30 (7), 2143–2156. https://doi.org/10.1029/94WR00586.

Niu, Z., He, H., Zhu, G., Ren, X., Zhang, L., Zhang, K., Yu, G., Ge, R., Li, P., Zeng, N., Zhu, X., 2019. An increasing trend in the ratio of transpiration to total terrestrial evapotranspiration in China from 1982 to 2015 caused by greening and warming. Agric. For. Meteorol. 279, 107701. https://doi.org/10.1016/j.agrformet.2019.107701.

Novick, K.A., Ficklin, D.L., Stoy, P.C., Williams, C.A., Bohrer, G., Oishi, A.C., Papuga, S.A., Blanken, P.D., Noormets, A., Sulman, B.N., Scott, R.L., Wang, L., Phillips, R.P., 2016. The increasing importance of atmospheric demand for ecosystem water and carbon fluxes. Nat. Clim. Chang. 6 (11), 1023–1027. https://doi.org/10.1038/nclimate3114.

Orth, R., Seneviratne, S.I., 2013. Propagation of soil moisture memory to streamflow and evapotranspiration in Europe. Hydrol. Earth Syst. Sci. 17, 3895–3911.

Peters, W., van der Velde, I.R., van Schaik, E., Miller, J.B., Ciais, P., Duarte, H.F., van der Laan-Luijkx, I.T., van der Molen, M.K., Scholze, M., Schaefer, K., Vidale, P.L., Verhoef, A., Wårlind, D., Zhu, D., Tans, P.P., Vaughn, B., White, J.W.C., 2018. Increased water-use efficiency and reduced CO2 uptake by plants during droughts at a continental scale. Nat. Geosci. 11, 744–748.

Priya, A.K., Muruganandam, M., Rajamanickam, S., Sivarethinamohan, S., Gaddam, M.K.R., Velusamy, P., Gomathi, R., Ravindiran, G., Gurugubelli, T.R., Muniasamy, S.K., 2023. Impact

https://doi.org/10.5194/egusphere-2026-5937
Preprint. Discussion started: 24 November 2026
© Author(s) 2026. CC BY 4.0 License.



of climate change and anthropogenic activities on aquatic ecosystem – A review. Environ. Res. 238, 117233.

Rahmati, M., Amelung, W., Brogi, C., Dari, J., Flammini, A., Bogena, H., Brocca, L., Chen, H., Groh, J., Koster, R.D., McColl, K.A., Montzka, C., Moradi, S., Rahi, A., Sharghi, F., Vanderborght, J., Vereecken, H., 2024. Soil moisture memory: State-of-the-art and the way forward. Rev. Geophys. 62 (2), e2023RG000828.

Raz-Yaseef, N., Yakir, D., Schiller, G., Cohen, S., 2012. Dynamics of evapotranspiration partitioning in a semi-arid forest as affected by temporal rainfall patterns. Agric. For. Meteorol. 157, 77–85.

Schlesinger, W.H., Jasechko, S., 2014. Transpiration in the global water cycle. Agric. For. Meteorol. 189–190, 115–117.

Schwalm, C.R., Anderegg, W.R.L., Michalak, A.M., Fisher, J.B., Biondi, F., Koch, G., Litvak, M., Ogle, K., Shaw, J.D., Wolf, A., Huntzinger, D.N., Schaefer, K., Cook, R., Wei, Y., Fang, Y., Hayes, D., Huang, M., Jain, A., Tian, H., 2017. Global patterns of drought recovery. Nature 548 (7666), 202–205.

Scott, R.L., Knowles, J.F., Nelson, J.A., Gentine, P., Li, X., Barron-Gafford, G.A., Bryant, R., Biederman, J.A., 2021. Water availability impacts on evapotranspiration partitioning. Agric. For. Meteorol. 297, 108251.

Shen, X., Bai, X., Zhao, C., Tan, Q., Luo, G., Li, C., Ran, C., Zhang, S., Xiong, L., Liao, J., Du, C., Li, Z., Xue, Y., Long, M., Li, M., Luo, Q., Yang, S., Zhang, X., Xie, Y., 2024. Global response of soil biodiversity to climate and land use changes. J. Clean. Prod. 471, 143381.

Shuttleworth, W.J., Gurney, R.J., 1990. The theoretical relationship between foliage temperature

https://doi.org/10.5194/egusphere-2026-5937
Preprint. Discussion started: 24 November 2026
© Author(s) 2026. CC BY 4.0 License.



and canopy resistance in sparse crops. Q. J. R. Meteorol. Soc. 116 (492), 497–519.

Shuttleworth, W.J., Wallace, J.S., 1985. Evaporation from sparse crops-an energy combination theory. Q. J. R. Meteorol. Soc. 111 (469), 839–855.

Strohmenger, L., Ackerer, P., Belfort, B., Pierret, M.C., 2022. Local and seasonal climate change and its influence on the hydrological cycle in a mountainous forested catchment. J. Hydrol. 610, 127914.

Su, H., Du, M., Liu, Q., Kang, X., Zhao, L., Zheng, W., Liao, Z., 2024. Assessment of regional ecosystem service bundles coupling climate and land use changes. Ecol. Indic. 169, 112844.

Wang, G., Ke, Q., Zhang, K., Li, Y., Liu, H., Yu, Y., Ma, Q., 2023. Responses of freeze-thaw process and hydrothermal variations within soil profiles to the cultivation of forest and grassland in Northeast China. Soil Tillage Res. 228, 105653. https://doi.org/10.1016/j.still.2023.105653.

Xu, M., Zhang, T., Zhang, Y., Chen, N., Zhu, J., He, Y., Zhao, T., Yu, G., 2021. Drought limits alpine meadow productivity in northern Tibet. Agric. For. Meteorol. 303, 108371.

Zhang, H., Liu, F., Zhang, J., 2022. Using composite system index to identify China's ecological and socio-economic transition zone. Front. Plant Sci. 13, 1057271.

Zhang, J., He, S., Li, Y., Xue, Y., 2026. Scale-dependent transition in soil moisture memory and its environmental controls in complex mountain terrain. Hydrol. Earth Syst. Sci. 30 (12), 3825–3851.

Zhang, J., Wu, Z., Li, Y., Qin, C., Cui, J., 2025. Memory character and predictive period of soil moisture in the root-zone and along hillslope. J. Hydrol. 660, 133428.

https://doi.org/10.5194/egusphere-2026-5937
Preprint. Discussion started: 24 November 2026
© Author(s) 2026. CC BY 4.0 License.



957 Zhao, W., Guo, Y., Jiang, Q., He, L., Xiao, Y., 2026. Refining the Shuttleworth-Wallace model with
958 particle swarm optimization and genetic algorithm for evapotranspiration simulation in the
959 ecotone of the eastern margin of the Tibetan Plateau. Catena 268, 110014.
960 Zhao, Z., Wu, Y., Chen, W., Liu, G., Tang, Y., Xue, S., 2024. Long-term vegetation succession
961 enhances the network complexity and stability of soil protozoan communities. Catena 245,
962 108346.
963 Zheng, C., Jia, L., Hu, G., Menenti, M., Timmermans, J., 2025. How much water vapour does the
964 Tibetan Plateau release into the atmosphere? Hydrol. Earth Syst. Sci. 29, 485–506.
965 Zhong, L., Ge, N., Ma, Y., Fu, Y., Ma, W., Han, C., Wang, X., Cheng, M., 2021. Estimation of land
966 surface latent heat flux over the Tibetan Plateau using geostationary satellite data. Adv. Earth
967 Sci. 36 (8), 773–784.